Inorganic Chemistry

Article

pubs.acs.org/IC

Pt···Pt vs Pt···S Contacts Between Pt-Containing Heterobimetallic Lantern Complexes

Frederick G. Baddour,[†] Stephanie R. Fiedler,[‡] Matthew P. Shores,[‡] Jeffrey W. Bacon,[†] James A. Golen,[§] Arnold L. Rheingold,[§] and Linda H. Doerrer*,[†]

[†]Department of Chemistry, Boston University, 590 Commonwealth Avenue, Boston, Massachusetts 02215, United States.

[‡]Department of Chemistry, Colorado State University, Fort Collins, Colorado 80523-1872, United States

[§]Department of Chemistry and Biochemistry, University of California, San Diego, 9500 Gilman Drive, MC 0332, La Jolla, California, 92093, United States

Supporting Information

ABSTRACT: A trio of Pt-based heterobimetallic lantern complexes of the form [(py)PtM(SAc)$_4$(py)] (M = Co, **1**; Ni, **2**; Zn, **3**) with unusual octahedral coordination of Pt(II) was prepared from a reaction of [PtM(SAc)$_4$] with excess pyridine. These dipyridine lantern complexes could be converted to monopyridine derivatives with gentle heat to give the series [PtM(SAc)$_4$(py)] (M = Co, **4**; Ni, **5**; Zn, **6**). An additional family of the form [PtM(SAc)$_4$(pyNH$_2$)] (M = Co, **7**; Ni, **8**; Zn, **9**) was synthesized from reaction of [PtM(SAc)$_4$(OH$_2$)] or [PtM(SAc)$_4$] with 4-aminopyridine. Dimethylsulfoxide and *N*,*N*-dimethylformamide were also determined to react with [PtM(SAc)$_4$] (M = Co, Ni), respectively, to give [PtCo(SAc)$_4$(DMSO)](DMSO), **10**, and [PtNi(SAc)$_4$(DMF)](DMF), **11**. Structural and magnetic data for these compounds and those for two other previously published families, [PtM(tba)$_4$(OH$_2$)] and [PtM(SAc)$_4$(L)], L = OH$_2$, pyNO$_2$, are used to divide the structures among three distinct categories based on Pt···Pt and Pt···S distances. In general, the weaker donors H$_2$O and pyNO$_2$ seem to favor metallophilicity and antiferromagnetic coupling between 3d metal centers. When Pt···S interactions are favored over Pt···Pt ones, no coupling is observed and the pK_a of the pyridine donor correlates with the interlantern S···S distance. UV−vis−NIR electronic and ^{1}H NMR spectra provide complementary characterization as well.

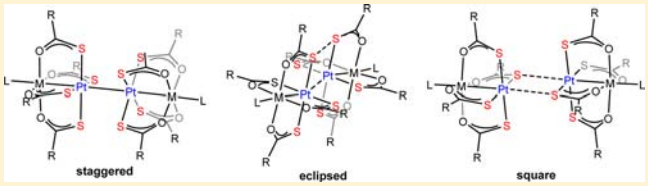

INTRODUCTION

Compounds with metal−metal bonding[1] are intellectually enticing to the inorganic chemist because they exhibit structural complexity and diversity beyond that available in nonmetals and also have seemingly limitless potential for application in materials from bulk to nano in scale. Early work emphasized the synthetically straightforward homometallic species in dimers and clusters.[1] Chemists have been particularly prolific with lantern (or paddlewheel) complexes of the general form [M$_2$(LX)$_4$(Y)$_n$], n = 0, 1, 2, with approximate D_{4h} symmetry, monoanionic chelating LX ligands and neutral or anionic axial donors Y, and a variety of metal−metal interactions depending on metal electron configuration. More recently, heterobimetallic dimers and clusters have begun to blossom as the need for differential metal behavior in many contexts,[2−9] such as multielectron processes in small molecule chemistry,[10−15] has become apparent. Heterobimetallic lantern complexes have similarly begun to evolve as their more sophisticated syntheses are elucidated.[16] Heterobimetallic complexes can combine the interesting physical properties that arise from metal−metal bonding, such has high electrical conductivity[17] and strong magnetic communication,[18−20] with the ability to tune the degree of electronic anisotropy that results from different metal centers in communication.

Previously, we reported[21] the synthesis and characterization of several families of heterobimetallic lantern complexes constructed with thiocarboxylate ligands of the form [PtM(SOCR)$_4$(L)] (R = Ph; M = Fe, Co, Ni; L = OH$_2$[22] and R= CH$_3$; M = Co, Ni, Zn; L = OH$_2$, pyNO$_2$[21]). Many of these complexes exhibited Pt···Pt metallophilic contacts in the solid state, which are defined as less than the sum of two Pt van der Waals radii (3.44 Å). In all paramagnetic cases except for M = Fe unpaired spins on the 3d metal are able to antiferromagnetically couple to diamagnetic ground states through these metallophilic interactions. Herein we report a detailed analysis of the profound effect substitution of the 3d-metal-bound axial ligand can have on formation of short Pt···Pt contacts.

EXPERIMENTAL SECTION

General Information. Potassium tetrachloroplatinate (K$_2$PtCl$_4$) was prepared using a combination of literature preparations: Hexachloroplatinic acid (H$_2$PtCl$_6$) was prepared[23] from commercially obtained platinum metal and converted to K$_2$PtCl$_6$ using a literature preparation,[19] and K$_2$PtCl$_4$ was synthesized from prepared K$_2$PtCl$_6$ using literature methods.[24] Precursors [PtNi(SAc)$_4$(OH$_2$)], PtCo(SAc)$_4$(OH$_2$)], and [PtZn(SAc)$_4$(OH$_2$)] and their anhydrous analogs

Received: August 12, 2013
Published: November 19, 2013

   dx.doi.org/10.1021/ic402075y | Inorg. Chem. 2013, 52, 13562−13575

were prepared as previously reported.[21] All other reagents were obtained commercially and used without further purification. Elemental analyses were performed by Atlantic Microlab Inc. (Norcross, GA). Thermogravimetric analysis (TGA) data were collected on a TA Instruments Q50 thermogravimetric analyzer. Typical data collection parameters include a heating rate of 10 °C/min and final temperature of 300 °C. UV−vis−NIR spectra were measured between 190 and 1500 nm with a Shimadzu UV-3600 spectrometer. ^{1}H NMR and ^{13}C{^{1}H} spectra measurements were recorded on a Varian 500 MHz spectrometer or Varian 400 MHz spectrometer.

*Synthetic Procedures. [(py)PtCo(SAc)$_4$(py)], **1**.* A portion of the insoluble gray powder [PtCo(SAc)$_4$] (52.3 mg, 0.09 mmol) was mixed with about 15 mL of pyridine and heated to 77 °C resulting in a clear pink solution. Upon complete dissolution of [PtCo(SAc)$_4$], in about 30 min the heat source was removed and the solution was allowed to evaporate slowly under ambient conditions. Pink crystals grown for X-ray analysis were grown within 3 days and filtered from the supernatant and washed with cold pyridine. Crystals were dried in vacuo for 6 h. Yield 69% (67 mg). Anal. Calcd for PtCoC$_8$H$_{12}$O$_4$S$_4$·1.6 C$_5$H$_5$N: C, 28.58; H, 2.99; N, 3.40. Found: C, 28.40; H, 2.81; N, 3.32. (Loss of Pt-coordinated pyridine is facile; see TGA data below.) UV−vis−NIR (CH_2Cl_2) (λ_{max}, nm (ε_M, cm^{-1} M^{-1})): 258 (31 800), 385sh (320), 496 (100), 524 (54), 578 (20), 1275 (5). Evans method (CD_2Cl_2): 5.18 μ_B.

*[(py)PtNi(SAc)$_4$(py)], **2**.* A portion of [PtNi(SAc)$_4$] (83 mg, 0.150 mmol) was dispersed in approximately 10 mL of pyridine. The yellow insoluble product began to react, forming a clear green solution after heating to ∼80 °C for 30 min. Green crystals for X-ray analysis were grown from the reaction mixture slowly, allowing evaporation to occur over 3 days, separated via filtration, and washed with a small portion of pyridine. Crystals, recovered in 80% yield (86 mg), were dried under high vacuum for 5 h. Anal. Calcd for PtNiC$_{18}$H$_{22}$N$_2$O$_4$S$_4$: C, 30.35; H, 3.11; N, 3.93. Found: C, 30.65; H, 3.03; N, 3.98. UV−vis−NIR (CH_2Cl_2) (λ_{max}, nm (ε_M, cm^{-1} M^{-1})): 258 (37 400), 337 (2050), 469sh (9) 673 (10), 831 (2), 1172 (9). Evans method (CD_2Cl_2): 3.15 μ_B.

*[(py)PtZn(SAc)$_4$(py)], **3**.* A portion of the insoluble white powder [PtZn(SAc)$_4$] (101 mg, 0.180 mmol) was dispersed in approximately 5 mL of hot pyridine (∼80 °C). A clear yellow solution was formed and set aside to cool to room temperature. Large colorless crystals suitable for single-crystal X-ray analysis were grown from slow evaporation in 41% yield (53 mg). Anal. Calcd for PtZnC$_{18}$H$_{22}$N$_2$O$_4$S$_4$: C, 30.06; H, 3.08; N, 3.90. Found: C, 30.23; H, 3.01; N, 3.92. UV−vis−NIR (CH_2Cl_2) (λ_{max}, nm (ε_M, cm^{-1} M^{-1})): 258 (30 800). ^{1}H NMR (δ, ppm, {$CDCl_3$}): 8.95 (d, J = 4.50 Hz, 2H, Zn-*o*-NC$_5$H$_5$), 8.62 (d, J = 3.00 Hz, 2H, Pt-*o*-NC$_5$H$_5$), 7.98 (t, J = 7.50 Hz, 1H, Zn-*p*-NC$_5$H$_5$), 7.68 (t, J = 7.50 Hz, 1H, Pt-*p*-NC$_5$H$_5$), 7.59 (pseudo-t, J = 6.50 Hz, 2H, Zn-*m*-NC$_5$H$_5$), 7.29 (pseudo-t, J = 7.00 Hz, 2H, Pt-*m*-NC$_5$H$_5$), 2.41 (s, 12H, -CH$_3$) ^{13}C{^{1}H} NMR (δ, ppm, {$CDCl_3$}: 215.12 (s, SO(*C*)CH$_3$), 149.97, (s, Zn−C2 and Zn−C6), 149.73 (s, Pt−C2 and C6), 139.46 (s, Zn−C4), 136.13 (s, Pt−C4), 125.15 (s, Zn−C3 and C5), 123.89 (s, Pt−C3 and C5), 33.07 (s, −CH$_3$).

*[PtCo(SAc)$_4$(py)], **4**.* A portion of **1** (17 mg, 0.024 mmol) was heated to ∼100 °C for 4 h in air, resulting in formation of **4** in quantitative yield (by TGA). Purple crystals suitable for single-crystal X-ray analysis were grown from slow evaporation of a saturated CH_2Cl_2 solution. Anal. Calcd for PtCoC$_{13}$H$_{17}$NO$_4$S$_4$: C, 24.64; H, 2.70; N, 2.21. Found: C, 24.49; H, 2.81; N, 2.09. UV−vis−NIR (CH_2Cl_2) (λ_{max}, nm (ε_M, cm^{-1} M^{-1})): 258 (28 300), 385sh (300), 497 (96), 523 (49), 573 (17), 1284 (4). Evans method (CD_2Cl_2): 4.61 μ_B.

*[PtNi(SAc)$_4$(py)], **5**.* A portion of **2** (64 mg, 0.090 mmol) was heated to ∼100 °C for 4 h in air, resulting in formation of **5** in quantitative yield (by TGA). Green crystals suitable for single-crystal X-ray analysis were grown from slow evaporation of a saturated CH_2Cl_2 solution. Anal. Calcd for PtNiC$_{13}$H$_{17}$NO$_4$S$_4$: C, 24.65; H, 2.71; N, 2.21. Found: C, 24.83; H, 2.77; N, 2.26. UV−vis−NIR (CH_2Cl_2) (λ_{max}, nm (ε_M, cm^{-1} M^{-1})): 258 (27 500), 463sh (13), 667 (11), 1169 (8). Evans method (CD_2Cl_2): 3.09 μ_B.

*[PtZn(SAc)$_4$(py)], **6**.* A portion of **3** (64 mg, 0.089 mmol) was heated to ∼93 °C for 3 h in air, resulting in formation of **6** in quantitative yield (by TGA). Colorless crystals suitable for single-crystal X-ray analysis were grown from slow evaporation of a saturated CH_2Cl_2 solution. Anal. Calcd for PtZnC$_{13}$H$_{17}$NO$_4$S$_4$: C, 24.40; H, 2.68; N, 2.19. Found: C, 24.55; H, 2.77; N, 2.20. UV−vis−NIR (CH_2Cl_2) (λ_{max}, nm (ε_M, cm^{-1} M^{-1})): 263(25 700). ^{1}H NMR (δ, ppm, {$CDCl_3$}): 8.94 (dt, J = 6.5 Hz, J = 1.5 Hz, 2H, *o*-NC$_5$H$_5$), 7.98 (tt, J = 8.0 Hz, J = 1.5 Hz, 1H, *p*-NC$_5$H$_5$), 7.59 (td, J = 6.5 Hz, J = 1.5 Hz, 2H, *m*-NC$_5$H$_5$), 2.41 (s, 12H, −CH$_3$) ^{13}C{^{1}H} NMR (δ, ppm, {$CDCl_3$}: 215.08 (s, SO(*C*)CH$_3$), 149.71 (s, C2 and C6), 139.44 (s, C4), 125.14 (s, C3 and C5), 33.07 (s, −CH$_3$).

*[PtCo(SAc)$_4$(pyNH$_2$)], **7**.* A slurry of [PtCo(SAc)$_4$] (200 mg, 0.361 mmol) in about 100 mL of DCM (CH_2Cl_2) was prepared, and solid pyNH$_2$ (68 mg, 0.721 mmol) was added. The reaction mixture was gently refluxed in air for about 4 h and concentrated to a volume of about 2 mL, resulting in a pastel purple precipitate. The solid was filtered off, washed with ethanol, and dried in vacuo. The solid was recovered in 64% yield (149 mg). Anal. Calcd for PtCoC$_{13}$H$_{18}$N$_2$O$_4$S$_4$: C, 24.07; H, 2.80; N, 4.32. Found: C, 23.96; H, 2.68; N, 4.23. UV−vis−NIR (CH_2Cl_2) (λ_{max}, nm (ε_M, cm^{-1} M^{-1})): 262 (24 100), 379sh (270), 504 (86), 525 (64), 1324 (5). Evans method ($CDCl_3$): 4.87 μ_B.

*[PtNi(SAc)$_4$(pyNH$_2$)], **8**.* Freshly prepared [PtNi(SAc)$_4$(OH$_2$)] (414 mg, 0.723 mmol) was dissolved in about 20 mL of acetone and added to about 180 mL of CH_2Cl_2. A 5 mL portion of DCM containing pyNH$_2$ (136 mg, 1.445 mmol) was also added; the reaction mixture was refluxed for 6 h and concentrated to about 5 mL of solvent, which caused a substantial amount of green precipitate to form. Approximately 50 mL of ethanol was added to this mixture, resulting in formation of additional precipitate. The solid was filtered off, washed with ethanol, and dried in vacuo. The solid was recrystallized from CH_2Cl_2 and ethanol, resulting in a 42% yield (196 mg). Anal. Calcd for PtNiC$_{13}$H$_{18}$N$_2$O$_4$S$_4$: C, 24.08; H, 2.80; N, 4.32. Found: C, 24.13; H, 2.66; N, 4.28. UV−vis−NIR (CH_2Cl_2) (λ_{max}, nm (ε_M, cm^{-1} M^{-1})): 249 (47 063), 333 (1844), 475sh (7), 678 (12), 1182 (9). Evans method ($CDCl_3$): 2.97 μ_B.

*[PtZn(SAc)$_4$(pyNH$_2$)], **9**.* Complex **9** was prepared in the same manner as [PtCo(SAc)$_4$(pyNH$_2$)] by employing [PtZn(SAc)$_4$]. A portion of [PtZn(SAc)$_4$] (200 mg, 0.357 mmol) was dispersed in ∼100 mL of CH_2Cl_2, and solid pyNH$_2$ (67 mg, 0.713 mmol) was added to the slurry. The reaction mixture was gently refluxed in air for about 3 h before filtering over a fine frit. Filtrate was concentrated to approximately 2 mL, and precipitation was forced by adding about 25 mL of ethanol. The white solid was filtered off, washed with ethanol, and dried in vacuo before being recovered in 77% yield (180 mg). Anal. Calcd for PtZnC$_{13}$H$_{18}$N$_2$O$_4$S$_4$: C, 23.84; H, 2.77; N, 4.28. Found: C, 23.84, H, 2.68; 4.25. UV−vis−NIR (CH_2Cl_2) (λ_{max}, nm (ε_M, cm^{-1} M^{-1})): 248 (63 700), 270 (sh, 42,800), 333 (sh, 1250). ^{1}H NMR (δ, ppm, {$CDCl_3$}): 8.48 (dd, J = 5.50 Hz, J = 1.50 Hz, 2H, *o*-NC$_5$H$_5$) 6.67 (dd, J = 5.50 Hz, J = 1.50 Hz, *m*-NC$_5$H$_5$), 4.52 (s, −NH$_2$), 2.40 (s, −CH$_3$) . ^{13}C{^{1}H} NMR (δ, ppm, {$CDCl_3$}): 214.82 (s, SO(*C*)CH$_3$), 152.45 (s, C4), 149.90 (s, C2 and C6), 109.79 (s, C3 and C5), 33.09 (s, −CH$_3$).

*[PtCo(SAc)$_4$(DMSO)](DMSO), **10**.* A portion of [PtCo(SAc)$_4$] (50 mg, 0.090 mmol) was added to 2 mL of DMSO that had been preheated to 63 °C. A homogeneous purple solution was obtained over the course of 30 min, which was concentrated to approximately 1 mL using strong air flow to accelerate evaporation, resulting in precipitation of purple crystalline solid. The mixture was cooled to 13 °C, and crystals were collected by filtration. Crystals were air dried for 3 h and under vacuum for about 22 h. Yield 53% (34 mg). Anal. Calcd for PtCoC$_{12}$H$_{24}$O$_6$S$_6$: C, 20.28; H, 3.40; N, 0.00. Found: C, 20.44; H, 3.25; N, 0.00. UV−vis−NIR (CH_2Cl_2) (λ_{max}, nm (ε_M, cm^{-1} M^{-1})): 266 (22 700), 504 (30), 527 (21), 572 (13), 1298(3). Evans method (CD_2Cl_2): 5.01 μ_B.

*[PtNi(SAc)$_4$(DMF)](DMF), **11**.* A portion of [PtNi(SAc)$_4$] (100 mg, 0.180 mmol) was dispersed in DMF, and the mixture was heated to ∼85 °C, forming a clear green solution within 30 min. Green single crystals were obtained in 39% yield (49 mg) via slow evaporation at room temperature. Anal. Calcd for PtNiC$_{14}$H$_{26}$N$_2$O$_6$S$_4$: C, 24.01; H,

Table 1. Summary of X-ray Crystallographic Data Collection Parameters

	1	2	3	4	5	6
formula	$C_{18}H_{22}CoN_2O_4PtS_4$	$C_{18}H_{22}N_2NiO_4PtS_4$	$C_{18}H_{22}N_2O_4PtS_4Zn$	$C_{13}H_{17}CoNO_4PtS_4$	$C_{13}H_{17}NNiO_4PtS_4$	$C_{13}H_{17}NO_4PtS_4Zn$
fw	712.64	712.42	719.08	633.54	633.32	639.98
cryst syst	monoclinic	monoclinic	monoclinic	triclinic	triclinic	triclinic
space group	*C*2/*c*	*C*2/*c*	*C*2/*c*	*P*-1	*P*-1	*P*-1
a, Å	9.7943(3)	9.7573(3)	9.7867(16)	8.4915(5)	8.6106(15)	8.5584(7)
b, Å	18.2314(7)	18.2019(5)	18.064(3)	10.6097(6)	10.4639(19)	10.5455(8)
c, Å	13.2080(5)	13.1832(3)	13.228(2)	11.6814(6)	11.5370(19)	11.6893(9)
α, deg	90.00	90.00	90.00	74.987(2)	76.692(5)	74.699(3)
β, deg	97.0950(1)	97.1200(1)	97.407(8)	76.199(2)	75.057(5)	75.693(3)
γ, deg	90.00	90.00	90.00	71.709(2)	72.423(6)	71.615(3)
V, Å^3	2340.41(15)	2323.30(11)	2319.0(7)	950.83(9)	944.3(3)	950.05(13)
Z	4	4	4	2	2	2
ρ(calcd), g cm^{-3}	2.022	2.037	2.060	2.213	2.227	2.237
μ, mm^{-1}	20.146 (Cu K*α*)	15.708 (Cu K*α*)	7.448 (Mo K*α*)	8.676 (Mo K*α*)	8.855 (Mo K*α*)	9.073 (Mo K*α*)
temp, K	100(2)	100(2)	90(2)	100(2)	100(2)	100(2)
R(*F*), %[a]	2.14	1.24	1.96	2.09	1.85	1.96
R(*ωF*^{2}), %[b]	5.29	3.03	4.90	4.54	4.17	4.74

	7	8	9	10	11
formula	$C_{13}H_{18}CoN_2O_4PtS_4$	$C_{13}H_{18}N_2NiO_4PtS_4$	$C_{13}H_{18}N_2O_4PtS_4Zn$	$C_{10}H_{18}CoO_5PtS$, C_2H_6OS	$C_{11}H_{19}NNiO_5PtS_4$, C_3H_7NO
fw	648.55	648.33	654.99	710.69	700.41
cryst syst	triclinic	triclinic	triclinic	triclinic	monoclinic
space group	*P*-1	*P*-1	*P*-1	*P*-1	$P2_1/c$
a, Å	8.8985(8)	8.8617(4)	8.9262(14)	8.6924(5)	13.0421(2)
b, Å	10.6574(1)	10.6957(4)	10.6627(17)	10.9949(6)	10.8041(2)
c, Å	11.0795(9)	11.0060(4)	11.0745(18)	12.2465(7)	17.1529(3)
α, deg	81.564(2)	81.9640(1)	81.620(7)	94.560(2)	90.00
β, deg	76.2150(1)	76.0040(1)	76.126(6)	93.722(2)	94.2780(1)
γ, deg	73.124(2)	73.1620(1)	72.970(7)	94.748(2)	90.00
V, Å^3	973.11(15)	966.07(7)	975.2(3)	1159.70(11)	2410.25(7)
Z	2	2	2	2	4
ρ(calcd), g cm^{-3}	2.213	2.229	2.231	2.035	1.930
μ, mm^{-1}	8.482 (Mo K*α*)	8.659 (Mo K*α*)	8.843 (Mo K*α*)	21.995 (Cu K*α*)	15.183 (Cu K*α*)
temp, K	100(2)	100(2)	90(2)	244(2)	292(2)
R(*F*), %[a]	1.45	1.60	2.10	5.19	2.47
R(*ωF*^{2}), %[b]	3.55	3.76	5.33	12.88	6.29

[a] $R = \sum||F_o| - |F_c||/\sum|F_o|$. [b] $R(wF^2) = \{\sum[\omega(F_o^2 - F_c^2)^2]\}/\{\sum[\omega(F_o^2)^2]\}^{1/2}$; $\omega = 1/[\sigma^2(F_o^2) + (aP)^2 + bP]$ with *a* and *b* given in CIF, $P = [2F_c^2 + \max(F_o,0)]/3$.

3.74; N, 4.00. Found: C, 24.07; H, 3.72; N, 3.99. UV−vis−NIR (CH_2Cl_2) (λ_{max}, nm (ε_M, cm^{-1} M^{-1})): 272 (25 100), 335 (1600), 493sh (5), 701 (8), 822 (4), 1319 (13). Evans method (CD_2Cl_2): 3.03 μ_B.

X-ray Crystallography. A summary of crystal data collection and refinement parameters for all compounds is found in Table 1. Crystals of **3**−**9** were mounted on a Cryoloop with Paratone-N oil, and data were collected at 90 or 100 K with a Bruker APEX II CCD using Mo K*α* radiation. Crystals of **1**, **2**, **10**, and **11** were mounted on a Cryoloop with Paratone-N oil, and data were collected at 100 K on a Bruker Proteum-R with a CCD detector using Cu K*α* radiation. Data were corrected for absorption with SADABS, and structures were solved by direct methods. All non-hydrogen atoms were refined anisotropically by full matrix least-squares on F^2. Hydrogen atoms H2NA and H2NB in complexes **7**−**9** were found from a Fourier difference map and allowed to refine isotropically with N−H distances of 0.87(2) Å and at 1.20 times U_{eq} of parent N atoms. All other hydrogen atoms were placed in calculated positions with appropriate riding parameters. A residual electron density of 1.22 e$^-$ was found 1.76 Å from H10A in complex **3** but was not resolvable. Sulfur (71.8/28.2%) and oxygen (46.7/53.3%) atoms were disordered over two positions in the structure of **6** and refined using a two-part model. Sulfur atoms were restrained with ISOR and oxygen atoms constrained with EADP.

Magnetic Measurements. Solution magnetic susceptibilities were determined with the Evans method[18] on a Varian 500 MHz spectrometer. Typical experimental conditions used a near-saturated solution of a prepared compound in acetone-d_6 doped with hexamethyldisiloxane and a capillary containing only acetone-d_6 doped with the same concentration of hexamethyldisiloxane.

Solid-state magnetic susceptibility data were collected with Quantum Design MPMS-XL (**1**, **2**, **4**, and **7**) and Quantum Design MPMS-5S (**5**, **8**, **10**, and **11**) SQUID magnetometers in the temperature range 2−300 K at an applied field of 1000 Oe. Microcrystalline samples were used as prepared without encasement in a polymer matrix. Samples were loaded into a gelcap or a sample pouch made from a small section of a drinking straw and sealed on both ends with an impulse sealer. The sealed pouch was inserted into a drinking straw as a sample holder and measured. Data were corrected for the holder and pouch magnetization by subtracting the susceptibility of an empty pouch and the holder straw and by subtracting the sample diamagnetic contributions calculated with Pascal's constants.[25] Theoretical fits to the susceptibility data of **2**, **5**, and **8** were generated using a relative error minimization routine (julX 1.4.1)[26] with a Hamiltonian of the form $H = DS_z^2 + E(S_x^2 + S_y^2)$. Fits to **1**, **4**, **7**, **10**, and **11** were attempted using julX and the same Hamiltonian and are presented in the Supporting Information. If necessary, refinements included a correction for temperature-

dx.doi.org/10.1021/ic402075y | *Inorg. Chem.* 2013, 52, 13562−13575

Scheme 1. Synthesis and TGA Behavior of 1−11

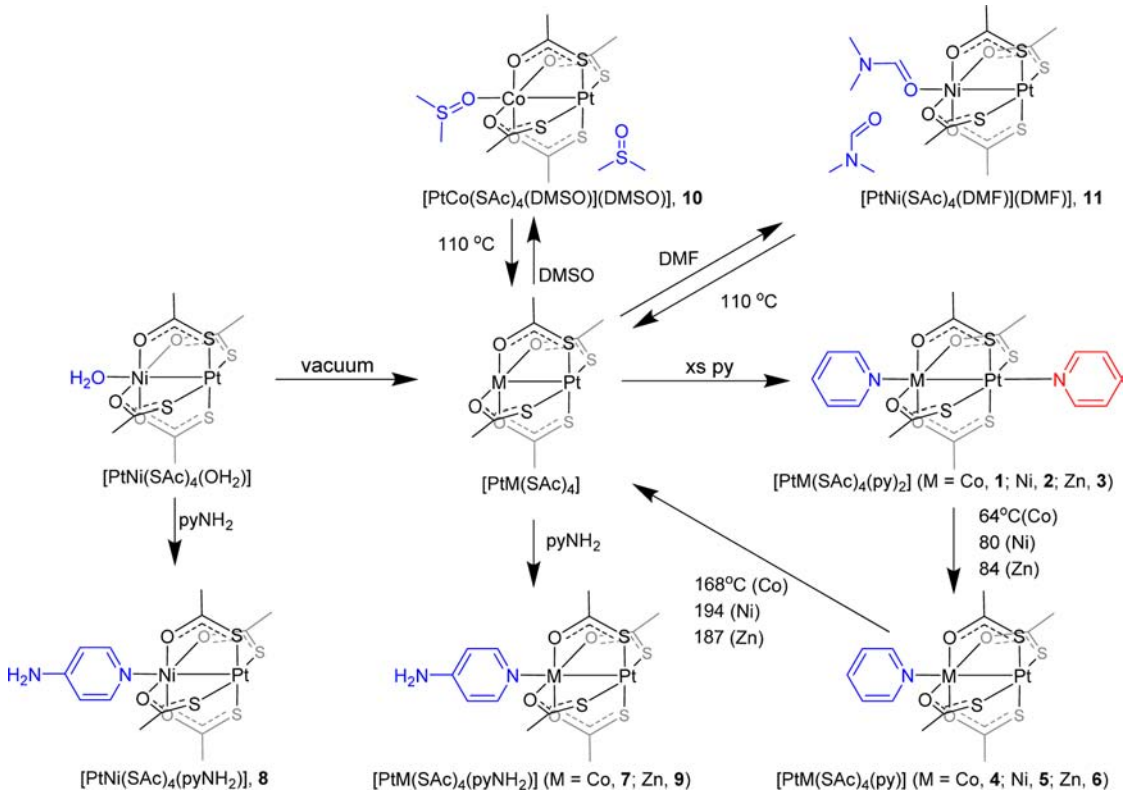

independent paramagnetism (TIP) and intermolecular (through a mean field approximation defined by julX as the parameter θ).

RESULTS AND DISCUSSION

Synthesis. We recently[21] showed the utility of the thioacetate ligand in the preparation of heterobimetallic lantern complexes with its two different binding moieties, S and O, allowing it to bind selectively platinum and first-row transition metals and minimize ligand exchange.

Compounds **1**−**3** were prepared by dispersing the insoluble $[PtM(SAc)_4]$ (M = Co, Ni, Zn) in an excess of warm pyridine to yield the dipyridine species, $[(py)PtM(SAc)_4(py)]$. The pyridine coordinated to the platinum center could be removed individually to generate the monopyridine species $[PtM(SAc)_4(py)]$ (M = Co, **4**; Ni, **5**; Zn, **6**) by heating to about 100 °C. The $[PtM(SAc)_4(pyNH_2)]$ (M = Co, **7**; Zn, **9**) pair could be prepared from a suspension of $[PtM(SAc)_4]$ in a CH_2Cl_2 solution of $pyNH_2$, whereas the Ni derivative, **8**, required the use of the more soluble $[PtNi(SAc)_4(OH_2)]$ to generate the analogous product. Compounds **10** and **11** were simply prepared by dispersing the insoluble $[PtM(SAc)_4]$ in warm DMSO and DMF, respectively, to yield $[PtM(SAc)_4L]L$ (M = Co, L = DMSO, **10**; M = Ni, L = DMF, **11**). All ligand addition and exchange reactions are shown in Scheme 1.

Compounds **1**−**3** reversibly coordinate two pyridine molecules as determined by X-ray crystallography and TGA, as shown in Scheme 1. The Co derivative, **1**, was determined to liberate 1 equiv of pyridine at 64 °C. The second equivalent of pyridine was not lost until the sample reached 168 °C. This large difference in the temperatures is due to the relative affinities of the metal ions for axial pyridine. Unsurprisingly, the pyridine coordinated to the platinum center is lost first as confirmed by recrystallization of the sample after heat treatment to 100 °C, which yields only the Co-coordinated monopyridine species, **4**. This result suggests that the pyridine bound to the Co center in **1** is more strongly bound and can be confidently assigned to the mass loss observed at 168 °C. If **1** is heated to between 168 °C and its decomposition temperature of 194 °C, the desolvated species $[PtCo(SAc)_4]$ is obtained (Scheme 1). Discrete loss of 2 equiv of pyridine at two widely separated temperatures is also observed in **2**, with the mass loss observed at 80 °C attributed to the Pt-coordinated pyridine to generate **5** and that at 194 °C assigned to loss of the Ni-coordinated pyridine. Compound **3** also exhibits this phenomenon, with the Pt-coordinated pyridine lost at 84 °C to form **6** and the Zn-coordinated pyridine lost at 187 °C. Compounds **1**−**3** can all be reconverted into their desolvated derivatives $[PtM(SAc)_4]$ by heating to a temperature between the temperature at which the second equivalent of pyridine is lost and their decomposition temperatures of 194, 253, and 256 °C, respectively. In contrast, upon similar heating, the aminopyridine adducts **7**−**9** show no evidence for liberation of the axially bound ligand. All three complexes are stable above 200 °C in the solid state, and no mass loss is observed before their decompositions noted at 239, 233, and 204 °C, respectively.

Compound **11** behaves similarly to the pyridine-coordinated species as each DMF molecule present in the crystal structure can be removed discretely by heating. The lattice solvent is liberated first at 95 °C followed by the Ni-coordinated DMF molecule being released at 110 °C. Two molecules of DMSO associated with **10** cannot be removed separately, however, and a mass loss equivalent to two molecules of DMSO is evident at 110 °C. All complexes prepared herein are quite thermally robust, with no decomposition of the metallic thioacetate core

dx.doi.org/10.1021/ic402075y | Inorg. Chem. 2013, 52, 13562−13575

Table 2. Selected Interatomic Distances and Angles

complex		distance (Å)		angle (deg)
1	Pt(1)−Co(1)	2.5817(6)	S(1)−Pt(1)−S(2)	90.01(3)
	Pt(1)−S(1)	2.3274(7)	S(1)−Pt(1)−S(1^{i})	177.97(3)
	Pt(1)−S(2)	2.3230(8)	S(2)−Pt(1)−S(2^{i})	179.38(3)
	Pt(1)−N(2)	2.567(4)	O(1)−Co(1)−O(2)	92.30(8)
	Co(1)−O(1)	2.106(2)	O(1)−Co(1)−O(1^{i})	179.33(8)
	Co(1)−O(2)	2.090(2)	O(2)−Co(1)−O(2^{i})	179.89(8)
	Co(1)−N(1)	2.106(4)	N(2)−Pt(1)−Co(1)	180.00(8)
			N(1)−Pt(1)−Co(1)	180.0(1)
2	Pt(1)−Ni(1)	2.5506(4)	S(1)−Pt(1)−S(2)	90.07(2)
	Pt(1)−S(2)	2.3221(5)	S(1)−Pt(1)−S(1^{i})	177.67(2)
	Pt(1)−S(1)	2.3246(5)	S(2)−Pt(1)−S(2^{i})	178.89(2)
	Pt(1)−N(2)	2.533(2)	O(1)−Ni(1)−O(2)	91.70(5)
	Ni(1)−O(2)	2.057(1)	O(1)−Ni(1)−O(1^{i})	177.69(5)
	Ni(1)−O(1)	2.067(1)	O(2)−Ni(1)−O(2^{i})	178.38(5)
	Ni(1)−N(1)	2.068(2)	N(1)−Ni(1)−Pt(1)	180.00(6)
			N(2)−Pt(1)−Ni(1)	180.00(5)
3	Pt(1)−Zn(1)	2.5313(7)	S(1)−Pt(1)−S(2)	89.87(4)
	Pt(1)−S(1)	2.3191(9)	S(1)−Pt(1)−S(1)#1	179.17(5)
	Pt(1)−S(2)	2.3206(10)	S(2)−Pt(1)−S(2)#1	177.84(5)
	Pt(1)−N(2)	2.476(4)	O(1)−Zn(1)−O(2)	87.96(9)
	Zn(1)−O(1)	2.143(2)	O(1)−Zn(1)−O(1)#1	177.73(13)
	Zn(1)−O(2)	2.154(2)	O(2)−Zn(1)−O(2)#1	177.39(13)
	Zn(1)−N(1)	2.085(4)	N(2)−Pt(1)−Zn(1)	180.00(8)
			N(1)−Zn(1)−Pt(1)	180.0(1)
4	Pt(1)−S(1)	2.3114(10)	S(1)−Pt(1)−S(4)	90.62(5)
	Pt(1)−S(4)	2.3160(10)	S(1)−Pt(1)−S(2)	88.79(5)
	Pt(1)−S(2)	2.3212(10)	S(4)−Pt(1)−S(2)	179.27(4)
	Pt(1)−S(3)	2.3240(9)	S(1)−Pt(1)−S(3)	178.78(4)
	Pt(1)−Co(1)	2.6298(5)	S(4)−Pt(1)−S(3)	90.02(4)
	Co(1)−O(1)	2.071(3)	S(2)−Pt(1)−S(3)	90.56(4)
	Co(1)−O(4)	2.076(3)	O(1)−Co(1)−O(4)	93.28(12)
	Co(1)−O(3)	2.084(3)	O(1)−Co(1)−O(3)	176.53(12)
	Co(1)−O(2)	2.093(3)	O(4)−Co(1)−O(3)	89.51(13)
	Co(1)−N(1)	2.101(3)	O(1)−Co(1)−O(2)	88.05(13)
	Pt(1)−S(2^{s})	3.0774(9)	O(4)−Co(1)−O(2)	177.60(12)
	Pt(1)−Pt(1^{s})	4.3042(3)	O(3)−Co(1)−O(2)	89.09(13)
			N(1)−Co(1)−Pt(1)	179.87(9)
			Co(1)−Pt(1)−Pt(1^{s})	133.03(1)
5	Pt(1)−S(4)	2.3127(9)	S(4)−Pt(1)−S(1)	90.04(3)
	Pt(1)−S(1)	2.3175(9)	S(4)−Pt(1)−S(3)	88.93(3)
	Pt(1)−S(3)	2.3200(9)	S(1)−Pt(1)−S(3)	178.78(3)
	Pt(1)−S(2)	2.3273(9)	S(4)−Pt(1)−S(2)	179.19(3)
	Pt(1)−Ni(1)	2.5831(6)	S(1)−Pt(1)−S(2)	90.62(3)
	Ni(1)−O(4)	2.040(2)	S(3)−Pt(1)−S(2)	90.42(3)
	Ni(1)−O(2)	2.049(2)	O(4)−Ni(1)−O(2)	178.48(9)
	Ni(1)−O(1)	2.052(2)	O(4)−Ni(1)−O(1)	91.29(9)
	Ni(1)−O(3)	2.062(2)	O(2)−Ni(1)−O(1)	89.80(9)
	Ni(1)−N(1)	2.059(3)	O(4)−Ni(1)−O(3)	88.95(9)
	Pt(1)−S(3s)	3.0587(9)	O(2)−Ni(1)−O(3)	89.96(9)
	Pt(1)−Pt(1s)	4.2308(6)	O(1)−Ni(1)−O(3)	179.75(10)
			N(1)−Ni(1)−Pt(1)	179.87(8)
			Ni(1)−Pt(1)−Pt(1s)	133.51(1)
6	Pt(1)−S(4)	2.317(3)	S(4)−Pt(1)−S(3)	90.29(9)
	Pt(1)−S(3)	2.318(3)	S(4)−Pt(1)−S(1)	90.41(9)
	Pt(1)−S(1)	2.325(3)	S(3)−Pt(1)−S(1)	178.33(10)
	Pt(1)−S(2)	2.325(3)	S(4)−Pt(1)−S(2)	178.63(9)
	Pt(1)−Zn(1)	2.6180(5)	S(3)−Pt(1)−S(2)	88.65(8)
	Zn(1)−N(1)	2.084(3)	S(1)−Pt(1)−S(2)	90.62(9)
	Zn(1)−O(3)	2.103(7)	O(3)−Zn(1)−O(4)	79.9(3)
	Zn(1)−O(4)	2.115(8)	O(4)−Zn(1)−O(1)	102.5(3)
	Zn(1)−O(1)	2.116(8)	O(3)−Zn(1)−O(2)	102.5(4)

dx.doi.org/10.1021/ic402075y | *Inorg. Chem.* 2013, 52, 13562−13575

Table 2. continued

complex		distance (Å)		angle (deg)
	Zn(1)−O(2)	2.134(6)	O(4)−Zn(1)−O(2)	177.5(2)
	Pt(1)−S(2s)	3.038(4)	O(1)−Zn(1)−O(2)	75.0(4)
	Pt(1)−Pt(1s)	4.2489(3)	O(3)−Zn(1)−O(1)	174.9(2)
			N(1)−Zn(1)−Pt(1)	179.55(8)
			Zn(1)−Pt(1)−Pt(1s)	133.35(1)
7	Pt(1)−S(1)	2.3184(6)	S(1)−Pt(1)−S(4)	89.03(2)
	Pt(1)−S(4)	2.3279(7)	S(1)−Pt(1)−S(3)	89.69(2)
	Pt(1)−S(3)	2.3283(7)	S(4)−Pt(1)−S(3)	178.46(2)
	Pt(1)−S(2)	2.3310(6)	S(1)−Pt(1)−S(2)	178.90(2)
	Pt(1)−Co(1)	2.6405(4)	S(4)−Pt(1)−S(2)	91.36(2)
	Co(1)−N(1)	2.072(2)	S(3)−Pt(1)−S(2)	89.93(2)
	Co(1)−O(4)	2.0752(18)	O(4)−Co(1)−O(3)	175.69(7)
	Co(1)−O(3)	2.0822(18)	O(4)−Co(1)−O(1)	90.46(7)
	Co(1)−O(1)	2.0843(17)	O(3)−Co(1)−O(1)	91.05(7)
	Co(1)−O(2)	2.0967(17)	O(4)−Co(1)−O(2)	90.13(7)
	Pt(1)−Pt(1s)	4.1224(3)	O(3)−Co(1)−O(2)	87.94(7)
	Pt(1)−S(3s)	3.2646(7)	O(1)−Co(1)−O(2)	173.95(6)
			N(1)−Co(1)−Pt(1)	177.81(6)
			Co(1)−Pt(1)−Pt(1s)	142.51(1)
8	Pt(1)−S(3)	2.3168(7)	S(3)−Pt(1)−S(4)	89.57(2)
	Pt(1)−S(4)	2.3240(7)	S(3)−Pt(1)−S(2)	89.20(2)
	Pt(1)−S(2)	2.3252(7)	S(4)−Pt(1)−S(2)	178.05(2)
	Pt(1)−S(1)	2.3294(7)	S(3)−Pt(1)−S(1)	179.19(2)
	Pt(1)−Ni(1)	2.5951(3)	S(4)−Pt(1)−S(1)	89.97(2)
	Ni(1)−N(1)	2.043(2)	S(2)−Pt(1)−S(1)	91.29(2)
	Ni(1)−O(2)	2.0485(18)	O(2)−Ni(1)−O(4)	178.45(7)
	Ni(1)−O(4)	2.0455(18)	O(2)−Ni(1)−O(3)	90.11(7)
	Ni(1)−O(3)	2.0481(17)	O(4)−Ni(1)−O(3)	91.23(7)
	Ni(1)−O(1)	2.0584(17)	O(2)−Ni(1)−O(1)	90.69(7)
	Pt(1)−Pt(1s)	4.1304(2)	O(4)−Ni(1)−O(1)	87.91(7)
	Pt(1)−S(4s)	3.2123(6)	O(3)−Ni(1)−O(1)	176.11(7)
			N(1)−Ni(1)−Pt(1)	178.51(6)
			Ni(1)−Pt(1)−Pt(1s)	140.34(1)
9	Pt(1)−S(1)	2.3177(10)	S(1)−Pt(1)−S(2)	89.81(4)
	Pt(1)−S(2)	2.3263(10)	S(1)−Pt(1)−S(4)	88.94(4)
	Pt(1)−S(4)	2.3280(10)	S(2)−Pt(1)−S(4)	178.45(3)
	Pt(1)−S(3)	2.3311(10)	S(1)−Pt(1)−S(3)	178.79(3)
	Pt(1)−Zn(1)	2.6617(6)	S(2)−Pt(1)−S(3)	89.76(4)
	Zn(1)−N(1)	2.047(3)	S(4)−Pt(1)−S(3)	91.50(4)
	Zn(1)−O(1)	2.097(2)	O(1)−Zn(1)−O(4)	90.58(10)
	Zn(1)−O(4)	2.102(3)	O(1)−Zn(1)−O(2)	91.38(10)
	Zn(1)−O(2)	2.108(3)	O(4)−Zn(1)−O(2)	174.19(10)
	Zn(1)−O(3)	2.116(2)	O(1)−Zn(1)−O(3)	172.19(10)
	Pt(1)−Pt(1s)	4.1406(6)	O(4)−Zn(1)−O(3)	90.04(10)
	Pt(1)−S(2s)	3.256(1)	O(2)−Zn(1)−O(3)	87.28(10)
			N(1)−Zn(1)−Pt(1)	177.77(9)
			Zn(1)−Pt(1)−Pt(1s)	142.10(1)
10	Pt(1)−Co(1)	2.6223(9)	S(4)−Pt(1)−S(3)	90.73(7)
	Pt(1)−S(4)	2.326(2)	S(4)−Pt(1)−S(1)	89.54(7)
	Pt(1)−S(3)	2.318(2)	S(4)−Pt(1)−S(2)	179.64(7)
	Pt(1)−S(1)	2.326(2)	S(3)−Pt(1)−S(1)	179.04(8)
	Pt(1)−S(2)	2.322(2)	S(3)−Pt(1)−S(2)	89.48(7)
	Co(1)−O(3)	2.095(5)	S(1)−Pt(1)−S(2)	90.25(7)
	Co(1)−O(5)	2.033(4)	O(4)−Co(1)−O(2)	176.6(2)
	Co(1)−O(4)	2.068(5)	O(3)−Co(1)−O(4)	90.4(2)
	Co(1)−O(2)	2.065(4)	O(3)−Co(1)−O(2)	90.6(2)
	Co(1)−O(1)	2.097(4)	O(3)−Co(1)−O(1)	174.8(2)
	Pt(1)−Pt(1s)	3.8489(3)	O(4)−Co(1)−O(1)	91.1(2)
	Pt(1)−S(1s)	3.225(2)	O(2)−Co(1)−O(1)	87.7(2)
			O(5)−Co(1)−Pt(1)	178.7(1)
			Co(1)−Pt(1)−Pt(1s)	146.38(2)

dx.doi.org/10.1021/ic402075y | *Inorg. Chem.* 2013, 52, 13562−13575

Table 2. continued

complex		distance (Å)		angle (deg)
11	Pt(1)−Ni(1)	2.5571(6)	S(4)−Pt(1)−S(2)	179.07(3)
	Pt(1)−S(4)	2.320(1)	S(4)−Pt(1)−S(3)	90.30(4)
	Pt(1)−S(2)	2.325(1)	S(4)−Pt(1)−S(1)	89.73(4)
	Pt(1)−S(3)	2.325(1)	S(2)−Pt(1)−S(3)	90.27(3)
	Pt(1)−S(1)	2.321(1)	S(2)−Pt(1)−S(1)	89.68(3)
	Ni(1)−O(2)	2.051(3)	S(3)−Pt(1)−S(1)	178.92(4)
	Ni(1)−O(4)	2.049(3)	O(2)−Ni(1)−O(4)	179.5(1)
	Ni(1)−O(3)	2.039(3)	O(2)−Ni(1)−O(3)	89.6(1)
	Ni(1)−O(1)	2.040(3)	O(2)−Ni(1)−O(1)	90.9(1)
	Ni(1)−O(1SL)	2.033(2)	O(4)−Ni(1)−O(3)	89.9(1)
	Pt(1)−Pt(1s)	4.2171(2)	O(4)−Ni(1)−O(1)	89.6(1)
	Pt(1)−S(2s)	3.0716(9)	O(3)−Ni(1)−O(1)	179.3(1)
			O(1SL)−Ni(1)−Pt(1)	178.74(8)
			Ni(1)−Pt(1)−Pt(1s)	135.14(1)

Table 3. Important Structural Factors for 1−11

formula	compound	Pt−M (Å)	Pt−L (Å, atom)	M−L (Å, atom)	angle of offset (deg)
$[(py)PtCo(SAc)_4(py)]$	**1**	2.5817(7)	2.567(4), N	2.106(4), N	NA
$[(py)PtNi(SAc)_4(py)]$	**2**	2.5506(4)	2.533(2), N	2.067(2), N	NA
$[(py)PtZn(SAc)_4(py)]$	**3**	2.5313(7)	2.476(4), N	2.085(4), N	NA
$[PtCo(SAc)_4(py)]$	**4**	2.6298(5)	3.0774(9), S	2.101(3), N	133.03(1)
$[PtNi(SAc)_4(py)]$	**5**	2.5831(6)	3.0587(9), S	2.5831(6), N	133.51(1)
$[PtZn(SAc)_4(py)]$	**6**	2.6180(5)	3.038(3), S	2.084(3), N	133.35(1)
$[PtCo(SAc)_4(pyNH_2)]$	**7**	2.6405(4)	3.2646(7), S	2.072(2), N	142.51(1)
$[PtNi(SAc)_4(pyNH_2)]$	**8**	2.5951(3)	3.2123(6), S	2.043(2), N	140.34(1)
$[PtZn(SAc)_4(pyNH_2)]$	**9**	2.5517(6)	3.256(1), S	2.047(3), N	142.10(1)
$[PtCo(SAc)_4(DMSO)](DMSO)$	**10**	2.6223(9)	3.225(2), S	2.068(5), O	146.38(2)
$[PtNi(SAc)_4(DMF)](DMF)$	**11**	2.5571(6)	3.0716(9), S	2.033(2), O	135.14(1)

at temperatures below 200 °C and most falling within 240−270 °C.

Structural Characterization. All compounds, **1**−**11**, have been crystallographically characterized, and data collection parameters are summarized in Table 1. Selected distances and angles are presented in Table 2, and a comparison of the most important lantern core metrical parameters is collected in Table 3.

Single-crystal X-ray diffraction studies of **1** reveal a lantern structure with a short Pt−Co distance of 2.5817(6) Å capped by two axially coordinated pyridine moieties, shown in Figure 1,

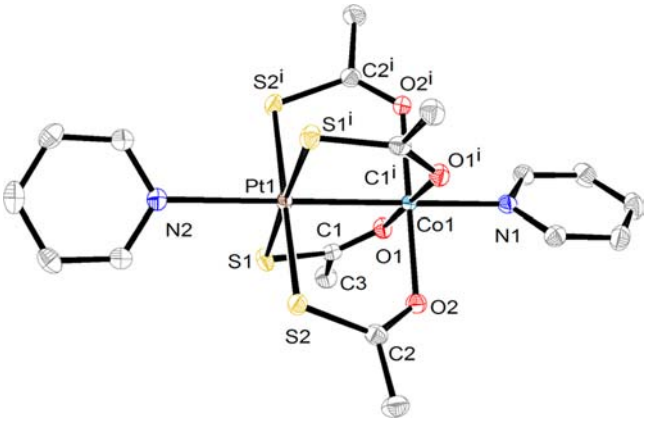

Figure 1. ORTEP of $[(py)PtCo(SAc)_4(py)]$, **1**. Ellipsoids are drawn at the 50% level. Superscript "i" indicates atoms related by a C_2 operation, and hydrogen atoms have been removed for clarity.

with a Co−N distance of 2.106(4) Å and an elongated Pt−N distance of 2.567(4) Å. This Pt−N_{py} contact is long compared to a more typical Pt(II)−N_{py} distance of 2.041(9) Å observed in *trans*-$[Pt(SCN)_2(py)_2]$.[27] A coordination number of six is rare for Pt(II) centers but has been observed in other cases with metal and nonmetal ligand atoms. Heteroleptic amidate compounds have Pt(II) with $\{Cl_4Pt(III)_2\}$ coordination[28] and $\{N_4ClRh(III)\}$[29] coordination. Several metallasilatrane complexes $[XSi(\mu\text{-mt})_4PtX]$ with mt = methimazolylsilane and X = halogen have been prepared that have octahedral coordination of Pt(II) by virtue of Pt(II) Lewis base donation to the Lewis acidic Si(IV) atom.[30−32] Divalent, six-coordinate Pt is also seen in a bis(phosphinoamide) species $[Pt(\eta^3\text{-}C_3H_4Me)\text{-}TiCl_2\{^tBuNP(Ph)_2\}_2]$,[33] and $[PtRh(tfepma)_2(CN^tBu)X_3]$ with tfepma = bis(trifluoroethoxyl)phosphinomethylamine formed after halogen oxidation with Pt(0) and Rh(I) precursors.[34] Six-fold coordination is more common for Pt(III) complexes,[35] such as $[Pt_2(OAc)_2(OH_2)_2](ClO_4)_2$[36] and $[Pt_2(OAc)_2(OH_2)_2](OTf)_2$,[37] and a homometallic Pt(III) analog of **1**−**3** has been structurally characterized[38] in $[Pt_2(H_2PO_4)(HPO_4)_3(py)_2]^-$, which exhibits axial Pt−N_{py} distances of 2.179(13) and 2.11(2) Å. Square planar Pt(II) accepts donation from an axial (fifth) ligand in complexes coordinated by 1,4,7-trithiacyclononane that engender heteroleptic square pyramidal coordination at the metal center.[39,40] Compounds **2** (Figure S1, Supporting Information) and **3** (Figure S2, Supporting Information) are isostructural to **1**, being pyridine-capped lantern complexes in the solid state with M−N distances of 2.068(2) and 2.086(4) Å and Pt−N distances of 2.533(2) and 2.477(4) Å, respectively. Observed

dx.doi.org/10.1021/ic402075y | *Inorg. Chem.* 2013, 52, 13562−13575

Pt−M distances for **2** and **3** are 2.5506(4) and 2.5313(7) Å, respectively.

Compound **4** is a monomeric lantern unit with a pyridine coordinated to the 3d metal site with a Co−N distance of 2.101(3) Å, indistinguishable from **1**. Unlike **1**, the platinum center of **4** is not terminated by an axial pyridine molecule (Figure 2, top). This open site allows the Pt center to form

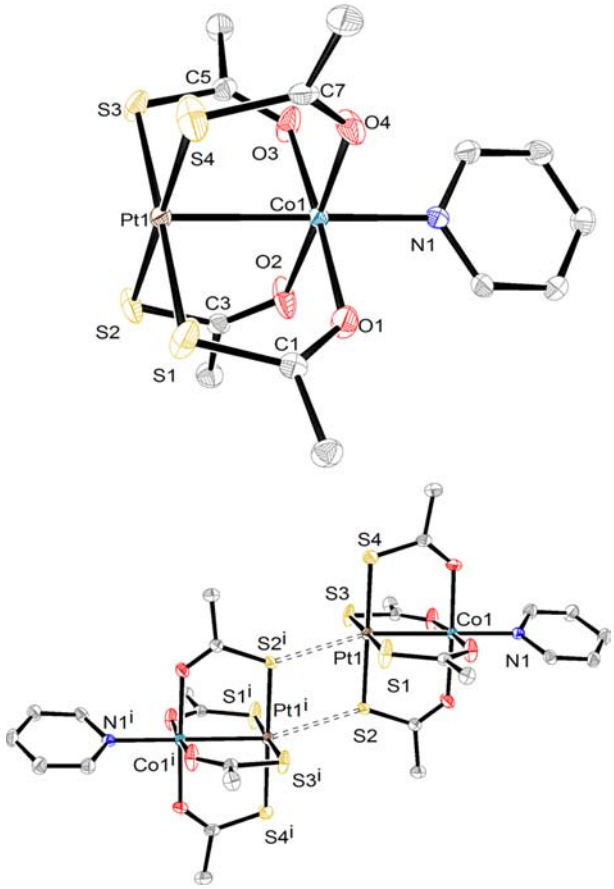

Figure 2. (Top) ORTEP of $[PtCo(SAc)_4(py)]$, **4**. (Bottom) Short intermolecular Pt···S contacts drawn between units of **4**. Ellipsoids are drawn at the 50% level. Superscript "i" indicates atoms related by a C_2 operation, and hydrogen atoms have been removed for clarity.

reciprocal, short intermolecular Pt···S contacts in the solid state with the nearest lantern unit creating a $\{Pt_2S_2\}$ square and dimer of slightly offset lantern units (Figure 2, bottom). The observed intermolecular Pt···S distance of 3.0774(9) Å is significantly less than the sum of the van der Waals radii for Pt and S (3.55 Å),[41] suggesting there is substantial stabilization resulting from formation of these Lewis acid−base interactions, which result in a large deviation of the adjacent Pt−M vectors from the linearity observed with Pt···Pt contacts.[21,22] The Co(1)−Pt(1)−Pt(1^i) angle in **4** is 133.03(1)°, as tabulated in Table 3 with other important structural data. The angle of offset of **4** results in a short intermolecular S···S contact between S2 and S2^i of 3.345(2) Å. Compound **5** is isostructural to **4**, with a Pt−Ni distance of 2.5831(6) Å and a Ni−N distance of 2.059(3) Å (Figure S3, Supporting Information, top). Molecules of **5** exhibit the same pairwise Pt···S contacts (Figure S3, Supporting Information, bottom) with a unique distance of 3.0587(9) Å, resulting in a similar Ni(1)−Pt(1)−Ni(1)^i angle of 133.51(1)° and two intermolecular S···S contacts of 3.476(1) and 3.402(1) Å. The Zn derivative, **6**, is also isostructural to **4**, with a Pt···Zn distance of 2.6180(4) Å and a Zn−N distance of 2.084(3) Å (Figure S4, Supporting Information, top). The Zn(1)−Pt(1)−Pt(1^i) angle is 133.35(1)° and the Pt···S distance is 3.038(3) Å (Figure S4, Supporting Information, bottom) with two intermolecular S···S contacts of 3.467(7) and 3.350(6) Å. Only three other examples of this platinum-containing lantern complex offset packing with short Pt···S contacts have been reported in the literature including two examples from our thiobenzoate series[22] $[PtM(tba)_4(OH_2)]$ in which M = Fe, Co (when recrystallized from CH_2Cl_2). The only additional example of such a short Pt···S contact in the solid state was observed for a {PtCr} heterobimetallic lantern complex assembled with the 4-methyl-pyridine-2-thiolato ligands in which intermolecular Pt···S distances of 2.888(3) and 3.304(5) Å were noted.[16] The square packing motif is much less common for homometallic platinum lantern complexes, which more frequently exhibit metallophilic interactions.[42,43] For example, among the seven $[Pt_2(S_2CR)_4]$ compounds[42−46] structurally characterized to date, only in one form of the acetate[47] and one form of the isobutanoate[46] is the Pt···S interaction favored over the Pt···Pt one. The other $[Pt_2(S_2CCH_3)_4]$[43] and $[Pt_2(S_2CC_3H_7)_4]$ structures belong to the group of seven that have an average metallophilic Pt···Pt distance of 3.19(8) Å and very weakly interacting Pt···S distance of 3.90(6) Å.

Compounds **7**−**9** are also monomeric lanterns with the 3d metal axially coordinated to a substituted pyridine, $pyNH_2$, and similar in structure to **4**−**6** except for a notable elongation of all Pt−M distances as shown in Table 3. The structure of **7** (Figure 3, top) reveals a Pt−Co distance of 2.6405(4) Å and a Co(1)−N(1) distance of 2.072(2) Å. Individual lantern units of **7** form two reciprocal intermolecular Pt(1)···S(3)^i contacts of 3.2646(7) Å resulting in the now-familiar offset geometry (with respect to the CoPt···PtCo vector) and eclipsed (with respect to the carboxylate ligands) arrangement of the two interacting $\{PtS_4\}$ faces (Figure 3, bottom) with an offset angle between units of **7** of 142.51(1)°. The amino hydrogen atoms of $pyNH_2$ form hydrogen-bonding contacts with S atoms of two different adjacent lantern units at distances of 2.79(3) and 2.73(3) Å. The structure of **8** (Figure S5, Supporting Information, top) exhibits the longest Pt−M distance of the $pyNH_2$ derivatives with a Pt−Ni distance of 2.5951(3) Å and a Ni−N distance of 2.043(2) Å. Lanterns of **8** also align to form a $\{Pt_2S_2\}$ square (Figure S5, Supporting Information, bottom) with an intermolecular Pt(1)···S(4)^i distance of 3.2123(6) Å and a Ni(1)−Pt(1)−Pt(1)^i angle of 140.34(1)°. The same short contacts between the $-NH_2$ protons and two thiocarboxylate S atoms of two adjacent lantern units are evident in the structure of **8** with distances of 2.78(3) and 2.75(3) Å. The intramolecular Pt−M and M−N distances observed within **9** (Figure S6, Supporting Information, top) are intermediate between those of **7** and **8**, with a Pt(1)···Zn(1) distance of 2.6617(6) Å and a Zn(1)−N(1) distance of 2.046(3) Å. Again, the lanterns of **9** are offset similarly to **7** and **8**, with a Zn(1)−Pt(1)−Pt(1)^i angle of 142.10(1)° and reciprocal intermolecular Pt(1)···S(2)^i distances of 3.256(1) Å. Two unique hydrogen-bonding interactions between the amine H atoms and thiocarboxylate S atoms of adjacent lanterns are also noted at distances of 2.70(5) and 2.76(3) Å. Hydrogen-bonding interactions involving the $-NH_2$ protons for **7**−**9** are shown in Figure S7, Supporting Information.

dx.doi.org/10.1021/ic402075y | *Inorg. Chem.* 2013, 52, 13562−13575

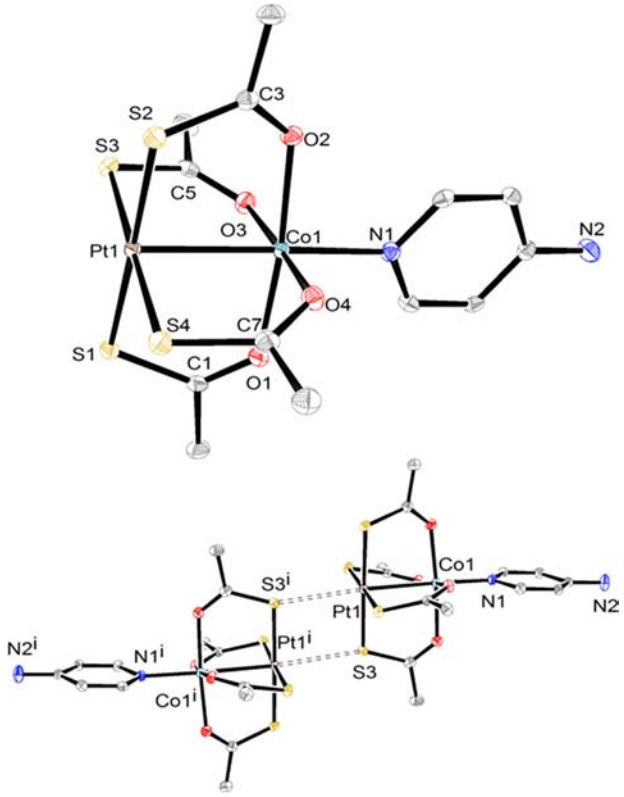

Figure 3. (Top) ORTEP of $[PtCo(SAc)_4(pyNH_2)]$, **7**. (Bottom) Short intermolecular Pt···S contacts drawn between units of **7**. Ellipsoids are drawn at the 50% level. Superscript "i" indicates atoms related by a C_2 operation, and hydrogen atoms have been removed for clarity.

Interestingly, the change from pyridine N-donor to solvent O-donor ligands results in the same offset alignment of lantern units. The intramolecular lantern structure of **10** is consistent with the other structures determined in this section, with a Pt–Co distance of 2.6223(9) Å. One equivalent of DMSO is bound to the cobalt center in the axial position through the oxygen atom with a Co–O distance of 2.033(4) Å, and 1 equiv of DMSO is present in the lattice. Compound **10** forms an offset dimer in the solid state with another pair of short Pt···S contacts of 3.225(2) Å as shown in Figure S8, Supporting Information. No short Pt···Pt contacts are formed as indicated by a $Co(1)–Pt(1)–Pt(1)^i$ angle of 146.38(2)°.

The observed Pt–Ni distance of 2.5571(6) Å is consistent with the range of Pt–Ni distances noted in Table 3. One equivalent of DMF is bound to the Ni center in **11** with a Ni–O distance of 2.033(2) Å, and 1 equiv of uncoordinated DMF is present in the lattice. Much like **10**, **11** forms an offset pair of lantern units through short, reciprocating intermolecular Pt···S contacts of 3.0716(9) Å as shown in Figure S9, Supporting Information. No short intermolecular Pt···Pt interactions are observed as a result of the square configuration, with the Pt centers of adjacent lanterns being misaligned as noted by a $Ni(1)–Pt(1)–Pt(1)^i$ angle of 135.14(1)°. This large angle of offset results in a close intermolecular S···S contact of 3.449(1) Å.

Several trends emerge from a comparative analysis of the structural parameters of compounds **1**–**9** as well as the $[PtM(tba)_4(OH_2)]$[22] and $[PtM(SAc)_4(OH_2)]$[21] series and $[PtM(SAc)_4(pyNO_2)]$ compounds,[21] and a list of important

Scheme 2. Structural Motifs in $[PtM(SOCR)_4(L)]$ Compounds

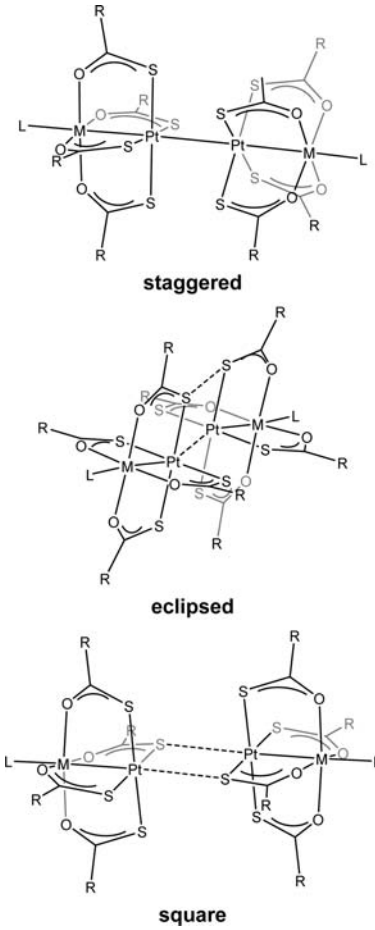

$[PtCo(tba)_4(OH_2)]$
$[PtNi(tba)_4(OH_2)]$
$[PtCo(SAc)_4(OH_2)]$
$[PtNi(SAc)_4(OH_2)]$
$[PtZn(SAc)_4(OH_2)]$
$[PtNi(SAc)_4(NO_2py)]$

$[PtCo(SAc)_4(NO_2py)]$
$[PtZn(SAc)_4(NO_2py)]$

$[PtFe(tba)_4(OH_2)]$
$[PtCo(SAc)_4(py)]$, **4**
$[PtNi(SAc)_4(py)]$, **5**
$[PtZn(SAc)_4(py)]$, **6**
$[PtCo(SAc)_4(pyNH_2)]$, **7**
$[PtNi(SAc)_4(pyNH_2)]$, **8**
$[PtZn(SAc)_4(pyNH_2)]$, **9**
$[PtCo(SAc)_4(DMSO)]$, **10**
$[PtNi(SAc)_4(DMF)]$, **11**

structural factors for the newest compounds is shown in Table 3. We categorize these structures in Scheme 2 as staggered, eclipsed, or square based on the M–Pt–Pt angles within pairs of lanterns and the resulting interactions between lantern structures. Most clear is that there is a group of compounds with virtually linear M–Pt–Pt angles with the shortest metallophilic Pt···Pt distances, ~3.1 Å, compared to the sum of two Pt van der Waals radii at 3.44 Å, based on the Bondi definition.[41,48] Accommodating such short Pt···Pt distances requires that the two lanterns be in a staggered conformation with respect to one another, which nevertheless allows S···S contacts as short as 3.5 Å. These two parameters are plotted in Figure 4 for all $[PtM(SOCR)_4(L)]$ compounds structurally characterized to date. Shorter S···S contacts < 3.5 Å and longer metallophilic distances ~3.4 Å were observed in $[PtCo(SAc)_4(pyNO_2)]$ and $[PtZn(SAc)_4(pyNO_2)]$,[21] which exhibit a largely eclipsed geometry between the two lantern moieties. Another large group of compounds has pairwise lantern interactions through two complementary Pt···S interactions that form a $\{Pt_2S_2\}$ square. This last group has a relatively narrow range of M–Pt–Pt angles but a wide range of interlantern S···S distances which depend primarily on the 3d M axial donor. In this family of square, pairwise interactions, there is a linear relationship between the M–Pt–Pt angle and the S···S distance because as the angle becomes more acute; the two S atoms are brought into closer contact as depicted in Scheme 3. Such dimerizations have also been seen in lanterns with RCO_2 carboxylates as well. A search of the Cambridge

dx.doi.org/10.1021/ic402075y | *Inorg. Chem.* 2013, 52, 13562–13575

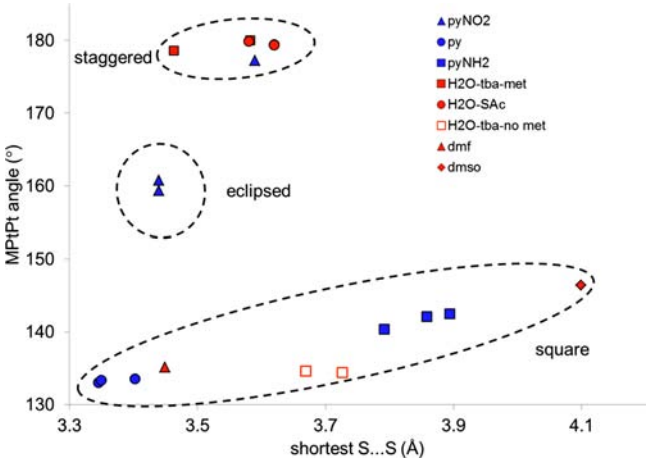

Figure 4. M−Pt−Pt angle versus shortest S···S distance in [PtM(SOCR)$_4$(L)] compounds and motif categorization.

Scheme 3. Illustration of Correlation Between M···Pt···Pt Angle in Blue and Intermolecular S···S Distance in Red

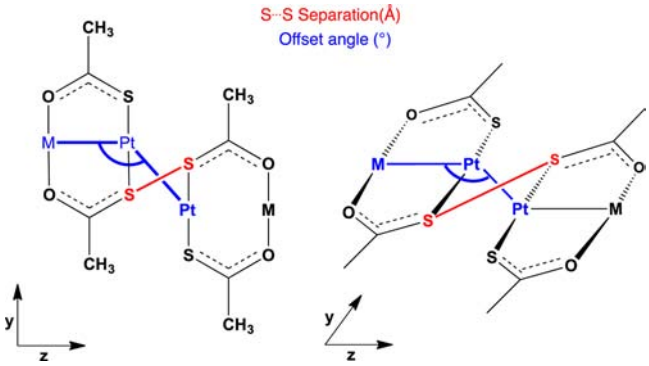

Structural Database,[49] v5.34, found 27 examples of the offset coordination mode that formed {M$_2$O$_2$} squares in 7 Fe$_2$ examples, 7 Cu$_2$, 13 Rh$_2$, and 1 CdPd case.

Because both O- and N-donor ligands have been studied and these three different types of structures have been observed, quantitative comparisons with definitive conclusions among all 17 structures are difficult. We therefore focus on compounds with pyridine derivatives bound to the 3d metal. There is generally a linear relationship between the M−N distance and the calculated[50] pK_a of the pyridine nitrogen as shown in Figure 5. The M−N distance decreases as the pyridine nitrogen becomes increasingly basic from pyNO$_2$ to py to pyNH$_2$. The shorter M−L bond is the result of more electron density donated from the pyridine nitrogen to the 3d$_{z^2}$ orbital. Notably, the Ni pyNO$_2$ derivative, does not fit this trend and exhibits the shortest M−N distance of the series. In the same compound there is an extraordinarily short Pt···Pt distance of 3.0794(6) Å between {PtNi} lantern units. Perhaps the diminished σ-donating ability of the pyridine nitrogen favors formation of a shorter Pt···Pt contact. The drastic shortening of the average Pt−Ni bond[21] of [PtNi(SAc)$_4$(pyNO$_2$)] (2.565(4) Å) could indicate better orbital overlap between Pt and Ni, resulting in better communication of ligand electronic effects to Pt. The other clear trend visible in Figure 5 is the correlation of M−L distance with the 3d metal such that for L = py, pyNH$_2$, pyNO$_2$, the Co−L distance is longest followed by Zn−L; and Ni−L is the shortest.

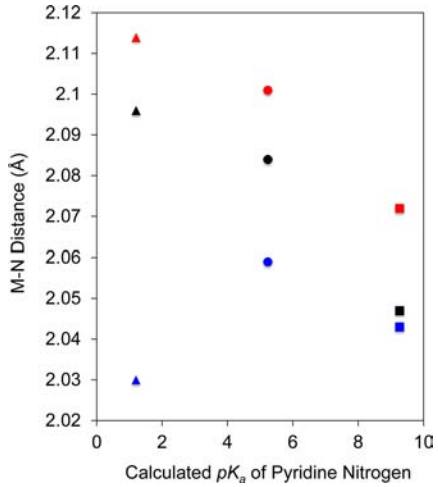

Figure 5. M−N distance of [PtM(SAc)(pyNO$_2$)] (M = Co, Ni, Zn) and **4**−**9** as a function of axial ligand pK_a: (red) {PtCo}, (blue) {PtNi}, (black) {PtZn}; (triangles) pyNO$_2$, (circles) py, (squares) pyNH$_2$.

The Pt−M distance is most strongly affected by the axial interactions at the Pt center. The Pt atoms in **1**−**9** all form close intra- or intermolecular contacts. In **1**−**3** Pt coordinates to pyridine, and in **4**−**9** the Pt centers form close contacts with a sulfur from an adjacent lantern complex in the square formation. As previously reported,[21] when the M(3d) coordinated to pyNO$_2$ short Pt···Pt metallophilic contacts form in the solid state. A qualitative trend emerges between the Pt···M and the Pt···L distances (Figure 6). As the Pt−L

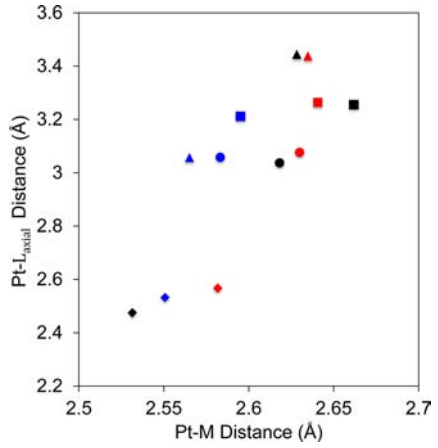

Figure 6. Pt−M distance as a function Pt−L distance of [PtM(SAc)$_4$pyNO$_2$] (M = Co, Ni, Zn) and **4**−**9**: (red) {PtCo}, (blue) {PtNi}, (black) {PtZn}; (triangles) pyNO$_2$, (circles) py, (squares) pyNH$_2$, (diamonds) py$_2$.

distance decreases, so decreases the Pt−M distance in an approximately linear fashion. This correlation suggests that axial ligand electron donation to the Pt center results in a net stabilization of the Pt−M σ orbital and a concomitant bond shortening, perhaps via enhanced Coulombic attraction between the metal centers. Previous DFT calculations[22] conducted on the series [PtM(tba)$_4$(OH$_2$)]$_2$ (M = Fe, Co, Ni) suggest that the 3d metal in these lantern structures has a significant positive charge because electron density is withdrawn by the thiobenzoate oxygen atoms. Further, the interaction between Pt and the 3d metal has donor (Pt)−

dx.doi.org/10.1021/ic402075y | Inorg. Chem. 2013, 52, 13562−13575

acceptor (M) character. Therefore, the relationship between the Pt−L distance and the Pt−M distance is the result of increasing the electron density at the Pt center, resulting in additional donation to 3d metal center.

A strong trans influence is not evident in the relationship between the Pt−M and the M−L distances, Figure 7. The

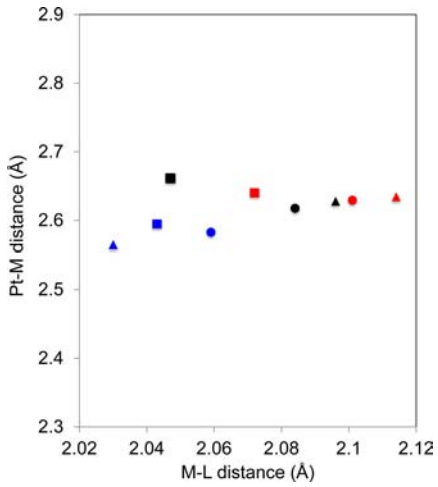

Figure 7. Pt−M distance as a function of M−L distance of $[PtM(SAc)_4pyNO_2]$ (M = Co, Ni, Zn) and **4**−**9**: (red) {PtCo}, (blue) {PtNi}, (black) {PtZn}; (triangles) $pyNO_2$, (circles) py, (squares) $pyNH_2$.

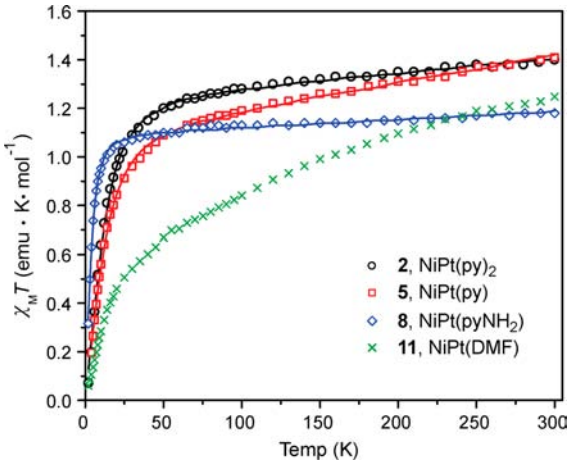

Figure 8. Variable-temperature magnetic susceptibility for nickel thioacetate lanterns, **2**, **5**, **8**, and **11**, measured in a 1000 Oe field. Best fits obtained from julX are shown as solid lines. In the absence of an acceptable fit for **11**, none is shown.

interplay between M−M bond distances and axial ligand σ-donor strength has been studied in great detail in many homometallic dinuclear species including rhodium, platinum,[51−56] and gold systems.[51] The structural trans influence in a Y−M−L unit causes M−L bond elongation trans to a trans-influencing ligand (Y). In the case of dinuclear Rh(III)−Rh(III) carboxylate species, the Rh−Rh bond is strongly trans influencing such that short Rh−Rh distances result in elongated $Rh-L_{axial}$ distances.[57] This effect has been attributed in large part to M−M σ-orbital stabilization, resulting in the M−L σ^* orbital (the orbital into which the axial ligands donate their electrons) destabilization and thus less effective bonding with respect to the axial ligand. The species herein exhibit very little change in the Pt−M distance when the σ-donor strength of the ligand coordinated to the 3d metal is changed as shown in Figure 7, suggesting that the Pt−M bonds are weaker trans influencers than the $Rh(III)_2$ bonds. Compounds **1**−**3** are the closest analogs to the previously studied dinuclear $[L-M(III)_2-L]^{n+}$ species, but modification of the pyridine to $pyNO_2$ or $pyNH_2$ in these $\{PtM(SAc)_4\}$ derivatives does not result in the binding of 2 equiv of the pyridine derivative, prohibiting a more detailed study of the structural trans influence.

There is no relationship between the Pt···Pt distance observed versus the pK_a of the 3d metal-bound axial ligand. Despite a general trend toward longer Pt···Pt distances as the pK_a of the axial ligand increases, the relationship is nonlinear. The relationship is confounded by the fact that Pt···Pt interactions have been supplanted by intermolecular Pt···S interactions in **4**−**9**, suggesting that there is competition between Pt···S and Pt···Pt intermolecular interactions, the strengths of which have not been ascertained. A related study of combinations among Au···Au, Au···S, and S···S interactions in dithiocarboxylates and xanthanates has been published,[58] which demonstrated the staggered and square configurations from Scheme 2, and addressed the eclipsed conformation computationally.

Magnetic Properties. Solution-phase magnetic susceptibilities for complexes **1**, **2**, **4**, **5**, **7**, **8**, **10**, and **11** were obtained by employing the Evans method.[18] The resultant effective magnetic moments of 5.18 (**1**), 4.61 (**4**), 4.87 (**7**), and 5.01 (**10**) all fall within the expected range[59] for monomeric {PtCo} species containing a high-spin Co(II) $S = 3/2$ in a pseudo-octahedral coordination geometry. The μ_{eff} values obtained for the Ni derivatives, 3.15 (**2**), 3.09 (**5**), 2.97 (**8**), 3.03 (**11**), are consistent with high-spin Ni(II) with oxygen donor ligands in a pseudo-octahedral coordination environment from the thiocarboxylate and axial ligands that results in an $S = 1$, monomeric {PtNi} species. Likewise, room-temperature solid-state magnetic susceptibility data for all paramagnetic species, obtained by SQUID magnetometry, are consistent with isolated $S = 3/2$ and 1 spin centers for Co(II)- and Ni(II)-containing complexes, respectively (Table 4).

Table 4. Room-Temperature Solid-State (300 K) and Solution Magnetic Susceptibilities

formula	compound	solution (Evans) μ_{eff}	solid state (SQUID) μ_{eff}
$[PtCo(SAc)_4(py)_2]$	**1**	5.18	5.04
$[PtNi(SAc)_4(py)_2]$	**2**	3.15	3.35
$[PtCo(SAc)_4(py)]$	**4**	4.61	4.97
$[PtNi(SAc)_4(py)]$	**5**	3.09	3.36
$[PtCo(SAc)_4(pyNH_2)]$	**7**	4.87	5.04
$[PtNi(SAc)_4(pyNH_2)]$	**8**	2.97	3.08
$[PtCo(SAc)_4(DMSO)](DMSO)$	**10**	5.01	5.18
$[PtNi(SAc)_4(DMF)](DMF)$	**11**	3.03	2.91

The temperature dependence of the susceptibility−temperature products for the Co-containing complexes is shown in Figure S10, Supporting Information. It is difficult to generate satisfactory fits for the magnetic data of the Co derivatives (**1**, **4**, **7**, and **10**) without resorting to complex expressions for magnetic anisotropy (zero-field splitting) and spin−orbit coupling typical for paramagnetic pseudo-octahedral Co(II)

dx.doi.org/10.1021/ic402075y | Inorg. Chem. 2013, 52, 13562−13575

Table 5. Comparison of Fitted Magnetic Parameters for {PtNi} Complexes

formula		g	$\|D\|$[a] (cm^{-1})	E/D	J (cm^{-1})	TIP (emu mol^{-1})	f[b]
$[PtNi(SAc)_4(py)_2]$	**2**	2.22	29.2	0.279	n/a	0.000580	0.01517
$[PtNi(SAc)_4(py)]$	**5**	2.09	30.3	0.333[c]	n/a	0.001100	0.01267
$[PtNi(SAc)_4(pyNH_2)]$	**8**	2.09	9.8	0.333[c]	n/a	0.000324	0.00787
$[PtNi(SAc)_4(H_2O)]$	ref 21	2.14	n/a	n/a	−50.8[d]	0.000500	0.0058
$[PtNi(SAc)_4(pyNO_2)]$	ref 21	2.04	n/a	n/a	−12.6[d]	0.000491	0.0059
$[PtNi(tba)_4(H_2O)]$	ref 22	2.19	n/a	n/a	−60[d]	0.001220	0.0039

[a]Sign of D is not determined by fitting susceptibility data. [b]Sum of the deviation squared. [c]Fixed parameter (not refined). [d]Data fit to a dimer model.

centers. It is clear from attempts to fit the data for the cobalt complexes **1**, **7**, and **10** and the nickel complex **11** using a spin-only model obtained from julX[26] that the complexes do not behave as "dimeric" $\{PtCo\}_2$ units as observed for $[PtM(tba)_4(OH_2)]$[22] or $[PtM(SAc)_4(pyNO_2)]$.[21] Similar fitting attempts for **7** using Magsaki (Figure S11, Supporting Information) are also consistent with the conclusion that modeling these complexes as $\{PtCo\}_2$ species yields nonsensical results. Data for Co-containing **4** are not readily fit by mono- or dimeric models, likely attributable to sample torquing; details are discussed in the Supporting Information.

In contrast, reasonable fits to the solid-state magnetic susceptibility data are obtained for Ni-containing complexes **2**, **5**, and **8** (Figure 8) using julX,[26] and the fitted magnetic parameters are tabulated in Table 5. As with the Co analogues, monomeric models are preferred for **2**, **5**, and **8**: dimeric models were attempted to compare the fit quality against the isolated monomer model, but in all cases the monomeric model gives a better fit to the data. At 300 K the $\chi_M T$ products for **2**, **5**, and **8** are 1.40, 1.41, and 1.18 emu K mol^{-1} (μ_{eff} = 3.35, 3.36, and 3.08 μ_B), respectively, which are slightly larger than what would be expected for an isolated Ni(II) center with $g = 2$ (1.00 emu K mol^{-1}). The low-temperature downturn of the $\chi_M T$ products of **2**, **5**, and **8** suggest zero-field splitting. The lack of significant intermolecular contacts observed in the crystal structures suggests that the intermolecular mean field approximation parameter (θ in julX) should be negligible. Note that inclusion of θ does not significantly improve the fits; in relation, substituting θ for anisotropy parameters gives poorer fits. Therefore, models excluding θ were used to avoid overparameterization. Details are provided in the Supporting Information.

Best-fit parameters for **2**, **5**, and **8** are presented in Table 5. We employ D here to improve the fit quality: models excluding D give significantly worse fits to the data. The counterpart to D, E (planar anisotropy), is therefore included as well. The D values obtained here and for preliminary Co(II) fits (see the Supporting Information) are relatively large compared to what is expected for first-row transition metals. When fitting **5** and **8**, free refinement gives $E/D > 3$, which is equivalent to redefining the molecular axes; therefore, E/D is fixed at 0.333. Note that attempts to fit the data for **5** as a dimer gives a small but nonzero J value, suggesting there may be some coupling between the monomers; however, the fit quality (f) for the monomer is better, and structural parameters (vide supra) support a monomer model. Similarly, fitting **8** as a monomer gives a good fit. Addition of a θ parameter suggests very little intermolecular interaction, and attempts to fit the data to a dimer model give a small J.

Note that an appropriate theoretical fit for the magnetic susceptibility data of **11** has not been obtained. Qualitatively, the temperature dependence of the $\chi_M T$ product is between the "monomeric" behavior of **2**, **5**, and **8** and the "dimeric" behavior of the thiobenzoate-ligated complexes disclosed previously,[17] possibly indicating that both single-ion anisotropy and intermolecular antiferromagnetic coupling are operative. In addition to possible coupling in **11**, attempts to fit **10** with julX (see the Supporting Information) suggest θ is important and that intermolecular coupling plays a role. Oxygen-containing compounds **10** and **11** are the only two species reported here that contain cocrystallized solvent molecules and which show factors indicative of antiferromagnetic coupling. We reason that the cocrystallized solvent may contribute to the intermolecular interactions, even without well-defined intermolecular contacts, e.g., hydrogen bonds.

Overall, solid- and solution-phase magnetic susceptibility data are internally consistent for both Co and Ni derivatives as shown in Table 4. The low-temperature downturns of the $\chi_M T$ values for all paramagnetic species reported here are consistent with zero-field splitting being dominant rather than antiferromagnetic coupling. These data suggest that the short Pt···S and S···S contacts observed in square structures do not facilitate an antiferromagnetic coupling interaction that has been observed when short Pt···Pt interactions exist between staggered or eclipsed lantern units.[21,22] In this way the lantern units **1**, **2**, **4**, **5**, **7**, and **8** are best considered as monomeric magnetic species, while **10** and **11** may contain some elements of intermolecular antiferromagnetic coupling.

Electronic Structure. Electronic spectra of compounds **1**–**11** are consistent with previous reports of thioacetate lantern complexes with homoleptic coordination around each metal center.[21,60] Co-containing complexes **1**, **4**, **7**, and **10** all exhibit three characteristic absorbances in the visible region near 495, 535, and 590 nm that can be attributed to d–d transitions on the Co center (Figure 9). There is only a minor perturbation in

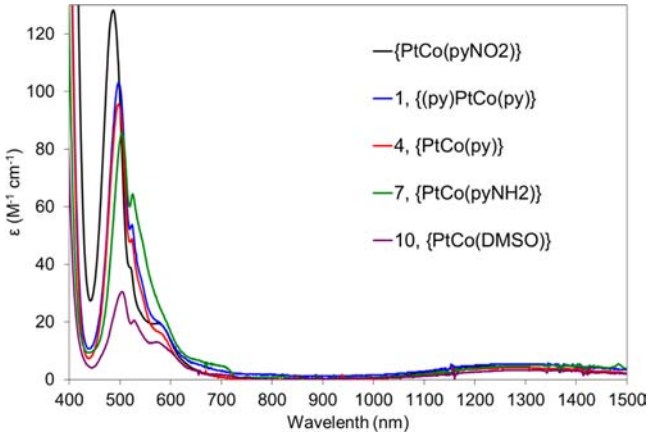

Figure 9. Vis–NIR spectra of Co derivatives $[PtCo(SAc)_4(pyNO_2)]$, **1**, **4**, **7**, and **10**.

dx.doi.org/10.1021/ic402075y | Inorg. Chem. 2013, 52, 13562–13575

Table 6. Vis−NIR Data of Co and Ni Derivatives

compound	λ, visible (nm) (CH_2Cl_2)	ε (cm^{-1}, M^{-1})	λ, near-IR (nm)	ε (cm^{-1}, M^{-1})
$[PtCo(SAc)_4(pyNO_2)]$	487	128	1233	5
$[(py)PtCo(SAc)_4(py)]$, **1**	496	103	1275	5
$[PtCo(SAc)_4(py)]$, **4**	497	96	1284	4
$[PtCo(SAc)_4(pyNH_2)]$, **7**	504	86	1324	5
$[PtCo(SAc)_4(DMSO)](DMSO)$, **10**	504	30	1298	3
$[PtNi(SAc)_4(pyNO_2)]$	660	10	1178	9
$[(py)PtNi(SAc)_4(py)]$, **2**	673	10	1172	9
$[PtNi(SAc)_4(py)]$, **5**	667	11	1169	8
$[PtNi(SAc)_4(pyNH_2)]$, **8**	678	12	1182	9
$[PtNi(SAc)_4(DMF)](DMF)$, **11**	701	8	1319	13

the energy and intensity of these absorptions as a function of axial pyridine substitution. A minor red shift and decrease of intensity of the most intense visible absorption feature is observed as the pyridine nitrogen becomes more basic as can be seen in Table 6. This red shift with axial ligand basicity is also observed for the NIR absorption bands attributed to an intermetallic d−d transition. Interestingly, the switch from N-donor pyridine derivatives to the O-donor DMSO does not result in a significant shift of the visible or NIR absorption bands; however, a significant decrease in the intensity of the major visible absorption is observed.

The same general trend holds for the Ni derivatives, **2**, **5**, **8**, and **11** (Figure 10); as the pyridine nitrogen becomes

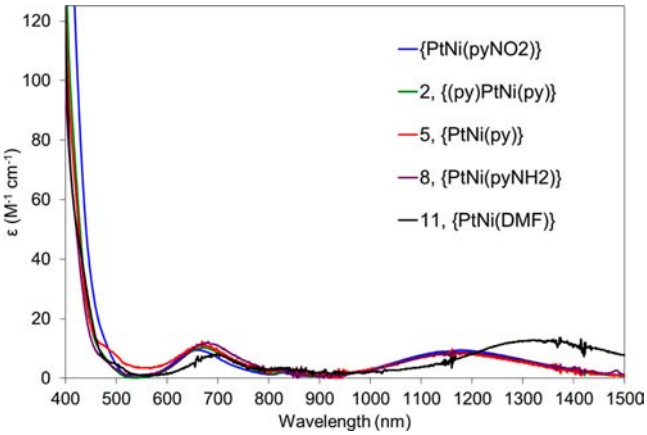

Figure 10. Vis−NIR spectra of Ni derivatives $[PtNi(SAc)4(pyNO_2)]$, **2**, **5**, **8**, and **11**.

increasingly basic from $pyNO_2$ to $pyNH_2$ there is a red shift of the major visible feature as clearly shown in Table 6. There appears to be no significant shift of the broad NIR absorbances as a function of the pyridine ligand; however, substituting the N-donor pyridine ligand for an O-donor DMF ligand results in a substantial shift in both the visible and the NIR absorbances. Unsurprisingly, none of the Zn compounds (**3**, **6**, **9**) exhibit visible or NIR absorbances, further supporting the proposal that the bands in the visible range originate from the 3d metal. Additionally, the NIR transitions that result from an intermetallic d−d transition in the Co and Ni derivatives between the Pt center and the 3d metal are not present in the Zn derivatives. The one transition in the diamagnetic thioacetate complexes which is found is a LMCT band that falls in the range 244−263 nm for all diamagnetic thioacetate complexes.

CONCLUSIONS

In summary, we prepared and thoroughly characterized eleven heterobimetallic lantern complexes with the core unit $[PtM(SOCR)_4(L)]$ (R = CH_3; M = Co, Ni, Zn). The $[(py)PtM(SOCR)_4(py)]$ complexes exhibit octahedral coordination for Pt(II) which is rare except for lantern and half-lantern complexes that facilitate this motif. Complexes $[PtM(SOCR)_4(L)]$ with square pyramidal Pt all form dimeric units in the solid state linked by intermolecular Pt···S interactions. These eight new structures were compared with other crystallographically characterized $[PtM(SOCR)_4(L)]$ compounds, and three structural categories are presented that are distinguished by their intermolecular (interlantern) Pt···Pt distances and the corresponding M···Pt···Pt angles. By systematically altering the axial ligand coordinated to the 3d metal center it was possible to establish other structural relationships as well. A correlation between the Pt−M and the Pt−L distances has been identified along with a dependence of the M−L distance on the pK_a of the coordinated pyridine nitrogen. The square structural motif observed here does not allow for magnetic exchange between lantern moieties, as observed from magnetic susceptibility data and fitting attempts.

ASSOCIATED CONTENT

Supporting Information

CIFs for **1**−**11**, ORTEP diagrams of **2**, **3**, **5**, **6**, **10**, and **11**; hydrogen-bonding interactions of **7**, **8**, and **9**; variable-temperature susceptibility plots for **1**, **4**, **7**, and **10**. This material is available free of charge via the Internet at http://pubs.acs.org.

AUTHOR INFORMATION

Corresponding Author

*E-mail: doerrer@bu.edu.

Notes

The authors declare no competing financial interest.

ACKNOWLEDGMENTS

We thank NSF-CCF 0829890 (LHD), NSF-CHE 0619339 (NMR spectrometer in the Chemical Instrumentation Center at Boston University), and NSF-CHE-1058889 (M.P.S.) and Colorado State University (SRF) for funding.

REFERENCES

(1) Cotton, F. A.; Murillo, C. A.; Walton, R. A. *Multiple Bonds Between Metal Atoms*; Springer: New York, 2005.

(2) Liu, S.; Motta, A.; Delferro, M.; Marks, T. J. *J. Am. Chem. Soc.* **2013**, *135*, 8830.

(3) Uyeda, C.; Peters, J. C. *Chem. Sci.* **2013**, *4*, 157.

(4) Jayarathne, U.; Mazzacano, T. J.; Bagherzadeh, S.; Mankad, N. P. *Organometallics* **2013**, *32*, 3986.
(5) Dutta, A.; Hamilton, G. A.; Hartnett, H. E.; Jones, A. K. *Inorg. Chem.* **2012**, *51*, 9580.
(6) Yow, S.; Gates, S. J.; White, A. J. P.; Crimmin, M. R. *Angew. Chem., Int. Ed.* **2012**, *51*, 12559.
(7) Filatov, A. S.; Napier, M.; Vreshch, V. D.; Sumner, N. J.; Dikarev, E. V.; Petrukhina, M. A. *Inorg. Chem.* **2012**, *51*, 566.
(8) West, N. M.; Labinger, J. A.; Bercaw, J. E. *Organometallics* **2011**, *30*, 2690.
(9) Hao, J.; Li, J.; Cui, C.; Roesky, H. W. *Inorg. Chem.* **2011**, *50*, 7453.
(10) Arnold, P. L.; Hollis, E.; Nichol, G. S.; Love, J. B.; Griveau, J.-C.; Caciuffo, R.; Magnani, N.; Maron, L.; Castro, L.; Yahia, A.; Odoh, S. O.; Schreckenbach, G. *J. Am. Chem. Soc.* **2013**, *135*, 3841.
(11) Yao, S.; Hrobarik, P.; Meier, F.; Rudolph, R.; Bill, E.; Irran, E.; Kaupp, M.; Driess, M. *Chem.—Eur. J.* **2013**, *19*, 1246.
(12) Maity, R.; Koppetz, H.; Hepp, A.; Hahn, F. E. *J. Am. Chem. Soc.* **2013**, *135*, 4966.
(13) Lacy, D. C.; Park, Y. J.; Ziller, J. W.; Yano, J.; Borovik, A. S. *J. Am. Chem. Soc.* **2012**, *134*, 17526.
(14) Teets, T. S.; Neumann, M. P.; Nocera, D. G. *Chem. Commun.* **2011**, *47*, 1485.
(15) Park, Y. J.; Ziller, J. W.; Borovik, A. S. *J. Am. Chem. Soc.* **2011**, *133*, 9258.
(16) Kitano, K. i.; Tanaka, R.; Kimura, T.; Tsuda, T.; Shimizu, S.; Takagi, H.; Nishioka, T.; Shiomi, D.; Ichimura, A.; Kinoshita, I.; Isobe, K.; Ooi, S. i. *J. Chem. Soc., Dalton Trans.* **2000**, 995.
(17) Chen, W.; Liu, F.; Nishioka, T.; Matsumoto, K. *Eur. J. Inorg. Chem.* **2003**, 4234.
(18) Evans, D. F. *J. Chem. Soc.* **1959**, 2003.
(19) Keller, R. N. *Inorg. Synth.* **1946**, *2*, 247.
(20) Phillips, V.; Baddour, F. G.; Lasanta, T.; López-de-Luzuriaga, J. M.; Bacon, J. W.; Golen, J. A.; Rheingold, A. L.; Doerrer, L. H. *Inorg. Chim. Acta* **2010**, *364*, 195.
(21) Baddour, F. G.; Fiedler, S. R.; Shores, M. P.; Golen, J. A.; Rheingold, A. L.; Doerrer, L. H. *Inorg. Chem.* **2013**, *52*, 4926.
(22) Dahl, E. W.; Baddour, F. G.; Fiedler, S. R.; Hoffert, W. A.; Shores, M. P.; Yee, G. T.; Djukic, J.-P.; Bacon, J. W.; Rheingold, A. L.; Doerrer, L. H. *Chem. Sci.* **2012**, *3*, 602.
(23) Kauffman, G. B. *Inorg. Synth.* **1967**, *9*, 182.
(24) Kauffman, G. B. *Inorg. Synth.* **1963**, *7*, 239.
(25) Bain, G. A.; Berry, J. F. *J. Chem. Educ.* **2008**, *85*, 532.
(26) Bill, E. *julX*. http://www.mpi-muelheim.mpg.de/bac/logins/bill/julX_en.php (Accessed 2008).
(27) Caira, M. R.; Nassimbeni, L. R. *Acta Crystallogr., Sect. B: Struct. Sci.* **1975**, *31*, 581.
(28) Matsumoto, K.; Arai, S.; Ochiai, M.; Chen, W.; Nakata, A.; Nakai, H.; Kinoshita, S. *Inorg. Chem.* **2005**, *44*, 8552.
(29) Uemura, K.; Yamasaki, K.; Fukui, K.; Matsumoto, K. *Eur. J. Inorg. Chem.* **2007**, *2007*, 809.
(30) Wagler, J.; Brendler, E. *Angew. Chem., Int. Ed.* **2010**, *49*, 624.
(31) Autschbach, J.; Sutter, K.; Truflandier, L. A.; Brendler, E.; Wagler, J. *Chem.—Eur. J.* **2012**, *18*, 12803.
(32) Autschbach, J.; Sutter, K.; Truflandier, L. A.; Brendler, E.; Wagler, J. *Chem.—Eur. J.* **2012**, *18*, 15903.
(33) Tsutsumi, H.; Sunada, Y.; Shiota, Y.; Yoshizawa, K.; Nagashima, H. *Organometallics* **2009**, *28*, 1988.
(34) Cook, T. R.; McCarthy, B. D.; Lutterman, D. A.; Nocera, D. G. *Inorg. Chem.* **2012**, *51*, 5152.
(35) Derek Woollins, J.; Kelly, P. F. *Coord. Chem. Rev.* **1985**, *65*, 115.
(36) Appleton, T. G.; Byriel, K. A.; Hall, J. R.; Kennard, C. H. L.; Mathieson, M. T. *J. Am. Chem. Soc.* **1992**, *114*, 7305.
(37) Appleton, T. G.; Byriel, K. A.; Garrett, J. M.; Hall, J. R.; Kennard, C. H. L.; Mathieson, M. T.; Stranger, R. *Inorg. Chem.* **1995**, *34*, 5646.
(38) Conder, H. L.; Cotton, F. A.; Falvello, L. R.; Han, S.; Walton, R. A. *Inorg. Chem.* **1983**, *22*, 1887.
(39) Grant, G. J.; Patel, K. N.; Helm, M. L.; Mehne, L. F.; Klinger, D. W.; VanDerveer, D. G. *Polyhedron* **2004**, *23*, 1361.
(40) Grant, G. J.; Pool, J. A.; VanDerveer, D. G. *Dalton Trans.* **2003**, 3981.
(41) Bondi, A. *J. Phys. Chem.* **1964**, *68*, 441.
(42) Pérez Paz, A.; Espinosa Leal, L. A.; Azani, M.-R.; Guijarro, A.; Sanz Miguel, P. J.; Givaja, G.; Castillo, O.; Mas-Ballesté, R.; Zamora, F. l.; Rubio, A. *Chem.—Eur. J.* **2012**, *18*, 13787.
(43) Guijarro, A.; Castillo, O.; Calzolari, A.; Miguel, P. J. S.; Gómez-García, C. J.; di Felice, R.; Zamora, F. l. *Inorg. Chem.* **2008**, *47*, 9736.
(44) Bellitto, C.; Bonamico, M.; Dessy, G.; Fares, V.; Flamini, A. *J. Chem. Soc., Dalton Trans.* **1987**, 35.
(45) Kawamura, T.; Ogawa, T.; Yamabe, T.; Masuda, H.; Taga, T. *Inorg. Chem.* **1987**, *26*, 3547.
(46) Bellitto, C.; Dessy, G.; Fares, V.; Flamini, A. *J. Chem. Soc., Chem. Commun.* **1981**, 409.
(47) Bellitto, C.; Flamini, A.; Piovesana, O.; Zanazzi, P. F. *Inorg. Chem.* **1980**, *19*, 3632.
(48) Alvarez, S. *Dalton Trans.* **2013**, *42*, 8617.
(49) Allen, F. H. *Acta Crystallogr., Sect. B: Struct. Sci.* **2002**, *58*, 380.
(50) Advanced Chemistry Development, Inc.: Toronto, Ontario, Canada, 2013; Version 11.02.
(51) Ling, S. S. M.; Puddephatt, R. J. *Polyhedron* **1986**, *5*, 1423.
(52) Cini, R.; Fanizzi, F. P.; Intini, F. P.; Natile, G. *J. Am. Chem. Soc.* **1991**, *113*, 7805.
(53) Che, C.-M.; Lee, W. M.; Mak, T. C. W.; Gray, H. B. *J. Am. Chem. Soc.* **1986**, *108*, 4446.
(54) Bandoli, G.; Dolmella, A.; Intini, F. P.; Pacifico, C.; Natile, G. *Inorg. Chim. Acta* **2003**, *346*, 143.
(55) Bandoli, G.; Caputo, P. A.; Intini, F. P.; Sivo, M. F.; Natile, G. *J. Am. Chem. Soc.* **1997**, *119*, 10370.
(56) Pacifico, C.; Intini, F. P.; Nushi, F.; Natile, G. *Bioinorg. Chem. Appl.* **2010**, *2010*, 1.
(57) Christoph, G. G.; Koh, Y. B. *J. Am. Chem. Soc.* **1979**, *101*, 1422.
(58) Azani, M.-R.; Castillo, O.; Gallego, M. L.; Parella, T.; Aullón, G.; Crespo, O.; Laguna, A.; Alvarez, S.; Mas-Ballesté, R.; Zamora, F. *Chem.—Eur. J.* **2012**, *18*, 9965.
(59) Cotton, F. A.; Wilkinson, G.; Murillo, C. A.; Bochmann, M. *Advanced Inorganic Chemistry*, 6th ed.; John Wiley & Sons, Inc.: New York, 1999.
(60) Melson, G. A.; Crawford, N. P.; Geddes, B. J. *Inorg. Chem.* **1970**, *9*, 1123.